THE JOURNAL OF PHYSICAL CHEMISTRY LETTERS
A JOURNAL OF THE AMERICAN CHEMICAL SOCIETY

pubs.acs.org/JPCL

Perspective

Higher-Order Multidimensional and Pump−Probe Spectroscopies

Julian Lüttig, Stefan Mueller, Pavel Malý, Jacob J. Krich, and Tobias Brixner*

Cite This: J. Phys. Chem. Lett. 2023, 14, 7556−7573

Read Online

ACCESS | Metrics & More | Article Recommendations

ABSTRACT: Transient absorption and coherent two-dimensional spectroscopy are widely established methods for the investigation of ultrafast dynamics in quantum systems. Conventionally, they are interpreted in the framework of perturbation theory at the third order of interaction. Here, we discuss the potential of higher-(than-third-)order pump−probe and multidimensional spectroscopy to provide insight into excited multiparticle states and their dynamics. We focus on recent developments from our group. In particular, we demonstrate how phase cycling can be used in fluorescence-detected two-dimensional spectroscopy to isolate higher-order spectra that provide information about highly excited states such as the correlation of multiexciton states. We discuss coherently detected fifth-order 2D spectroscopy and its power to track exciton diffusion. Finally, we show how to extract higher-order signals even from ordinary pump−probe experiments, providing annihilation-free signals at high excitation densities and insight into multiexciton interactions.

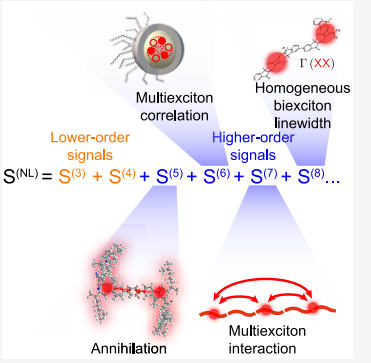

Ultrafast spectroscopy is employed to investigate phenomena on the time scale of femtoseconds, unraveling various physical properties. The most common technique is pump−probe (PP) spectroscopy, usually carried out in transient absorption geometry: A first pulse, often called the pump pulse, excites the system, while a second pulse (the probe pulse) detects the frequency-resolved transient change (in absorption) after a time delay T. In terms of perturbation theory, a conventional PP experiment probes the third-order polarization. An extension of PP is coherent two-dimensional (2D) spectroscopy, where third-order polarization is characterized as well but as a function of both excitation and detection frequency.[1,2] 2D spectra can be acquired, for example, by replacing the single excitation pulse from PP spectroscopy with two pump pulses with variable time delay τ. Fourier transformation over τ provides the excitation frequency axis while the detection frequency axis can be obtained directly by a spectrometer via measuring the spectral interference of the signal with a "local oscillator" (LO) pulse that may be either a separate reference pulse that does not interact with the sample or the probe pulse itself.[3−5] Another option for obtaining detection frequency resolution is to replace the spectrometer with a single-channel detector and to vary systematically the time delay between the signal and the LO, performing a numerical Fourier transformation.[6−8] We refer to PP and 2D spectroscopy in the described detection schemes as "coherently detected techniques" because interference between the signal field and another pulse is utilized.[9] It is also possible to detect an incoherent observable,[10−24] such as fluorescence or photocurrent, which we refer to as "action-detected spectroscopy". Resonant excitations of the system appear as diagonal peaks on a 2D map. Cross peaks indicate coupling or energy transfer in coherently detected 2D spectroscopy[25,26] and energy transfer as well as exciton−exciton annihilation (EEA)[27,9,28] in "action-detected" 2D spectroscopy.[10−24] The evolution of the 2D spectrum as a function of delay T provides information about, for example, energy transfer,[29] wave packet dynamics,[30] and coherences,[31] while the analysis of the 2D line shapes can be used to determine the interaction of the system with its environment.[31,32] Nowadays, both techniques, PP and 2D spectroscopy, are well-established and frequently used to investigate artificial[33] or natural light-harvesting complexes,[29] supramolecular systems,[34] chemical reactions,[35] 2D materials,[36] semiconductor nanostructures,[37] and many more. Recent developments include the use of incoherent observables, such as fluorescence,[10−14] photoelectrons,[15−17] photoions,[18−20] or internal photocurrents,[21−24] to measure ultrafast dynamics.

Ultrafast spectroscopy usually relies on a perturbative description of light−matter interaction. In general, all of the higher-order terms of the perturbation series are present in any given experiment. The common practice to suppress unwanted higher orders is to choose the excitation intensities in such a way that higher-order signals do not contribute significantly, ideally, so they are below the noise floor of the measurement. For example, in a 2D experiment, the intensity of the pulses as

Received: June 21, 2023
Accepted: August 4, 2023

https://doi.org/10.1021/acs.jpclett.3c01694
J. Phys. Chem. Lett. 2023, 14, 7556−7573

well as the phase-matching condition can be set in such a way that the detected 2D signal is dominated by the third-order signal, and higher-order signals do not contribute significantly. For higher excitation intensities, the higher-order terms contribute more and more. This is well-known for excitonic systems for which at high excitation intensities, exciton−exciton annihilation mixes into the 2D and PP signals.[38,39] Especially in light-harvesting complexes, the uncontrolled mixing of EEA with the single-exciton dynamics has challenged researchers for years.[40,41] Annihilation can only be reduced by low-power measurements that in turn may lead to a low signal-to-noise ratio (SNR).[40] Alternatively, EEA has to be included in the data analysis to avoid misinterpretation, which complicates matters and requires an a priori model.[42] If a suitable model is available, however, EEA can be utilized in power-dependent PP studies to investigate exciton migration in extended systems such as light-harvesting complexes or molecular aggregates.[43−45] In such experiments, the third- and fifth-order signals (and even higher orders) are mixed together, making it difficult to disentangle the data. As we outline in the present Perspective, this problem can be solved using higher-order spectroscopy, which allows us to obtain separated higher-order signals. We will employ the term "higher order" for such signals that are at least of fifth order in the electric field in a perturbation-theory description, while the third and fourth orders are the "conventional lower-order" time-resolved methods using either coherent or incoherent detection, respectively.

Besides EEA, higher-order spectroscopy unveils system properties and dynamics that cannot be directly observed by lower-order techniques. Examples include coherences between highly excited electronic states in quantum wells,[46] multistep energy transfer in light-harvesting complexes,[47] and highly excited vibrational states.[48] Following the principle of 2D spectroscopy, higher-order signals can be obtained by adding additional interactions, each of them with its own associated pulse.[49] Scanning all time delays and performing Fourier transformations distribute the higher-order signal over multiple dimensions (four or more). Instead of using one pulse per interaction, other approaches rely on multiple interactions from the same pulse, inherently reducing the dimensionality of the obtained spectra.[46,50−52] The dimensionality can also be reduced by setting specific time delays to zero while retaining separate laser beams. For example, multiple population-period transient spectroscopy (MUPPETS) uses two pulses from different directions that interact with the system at the same time.[53] In general, the main challenge in higher-order spectroscopy is to separate the individual nonlinear orders and, at the same time, keep the experiment feasible as it is technically demanding to isolate weak higher-order signals in a multipulse experiment that requires scanning of multiple delays.

The Perspective is structured as follows: First, we analyze the technical approaches to isolate higher-order signals. Then, we demonstrate how various higher-order signals can be isolated from one single experiment in fluorescence-detected 2D spectroscopy using phase cycling. Next, we discuss coherently detected fifth-order 2D spectroscopy as a tool to investigate exciton diffusion in extended systems such as polymers. We further discuss the simulation of higher-order signals. Finally, we show how higher-order signals can be isolated in a simple PP experiment by systematically varying the excitation intensity. This new technique is straightforward to implement and isolates clean nonlinear orders.

Isolation of Higher-Order Signals in 2D Spectroscopy. In 2D spectroscopy, the different signal contributions can be labeled by their specific coherences that occur during various time delays. We distinguish, on the one hand, the so-called one- or multiquantum signals in multidimensional spectroscopy, which are the signals that appear at one or several times the laser frequency, respectively, and on the other hand the nonlinear-order signals, which are the contributions arising from the various terms of the perturbative expansion of the nonlinear response in powers of the electric field. While at first glance one might think that these two definitions are equivalent, they are in fact not, and the clarification of their relation is a main topic of the present Perspective.

We label the multiquantum signals in multidimensional spectroscopy as $XQYQZQ$ where X, Y, and Z correspond to the quanta of coherences [one-quantum (1Q), two-quantum (2Q), etc.] with respect to the laser central frequency ω_0 that evolve as a function of the time delays τ, T, and t, respectively. The (first) coherence time τ is defined as the delay between the two pump pulses, while the population time T is defined as the delay between pump and probe. The time t (the "second" coherence time, also called "signal time") is defined as the delay between the probe and the emission of the signal. The coherences during τ and t determine the position of the signal on the excitation and detection axis, respectively. It is also possible to isolate zero-quantum (0Q) coherences, which are superpositions between states within a particular manifold such as between two vibrational sublevels of a single-exciton state. We will use the label 0Q during the population time T to indicate that a population in a single manifold is present, which allows one to observe vibrational coherences as stated above, coherences between electronic states of the same manifold, as well as population dynamics. For example, in a typical "photon-echo-type" 2D experiment, one isolates the 1Q0Q1Q signal, which correlates one-quantum coherence during τ with one-quantum coherence during t, with the possibility of tracking population dynamics as well as coherences during time delay T. Sometimes the YQ label is omitted even if the population time is scanned to keep the notation simple.[54] We also discuss population-detected signals generated by three pulses. For such signals, only two delays are scanned (the coherence times τ and t), and accordingly we will label the multiquantum signals from three-pulse experiments as $XQZQ$ signals.[55]

Nonlinear signals are often discussed in the framework of double-sided Feynman diagrams.[6,56] In these diagrams, the density matrix is shown between two vertical lines and interaction with the electric field is shown as arrows pointing toward or away from the density matrix. Each diagram represents a pathway of the density matrix in time-dependent perturbation theory; the sum of all the diagrams' contributions gives the signal.[57,58] Time flows from the bottom to the top. Let us first focus on the diagrams of coherently detected experiments (Figure 1a). An arrow pointing to the left is connected to $-\mathbf{k}$, while an arrow pointing to the right represents an interaction with $+\mathbf{k}$. We depict the emission of the signal in coherently detected experiments by a dotted arrow, which formally arises from a dipole transition of the density matrix after it has evolved under the influence of the optical pulses. In action-detected experiments, we use a double wavy arrow to indicate signals arising from the population. In Figure 1a we present two examples of double-sided Feynman

https://doi.org/10.1021/acs.jpclett.3c01694
J. Phys. Chem. Lett. 2023, 14, 7556−7573

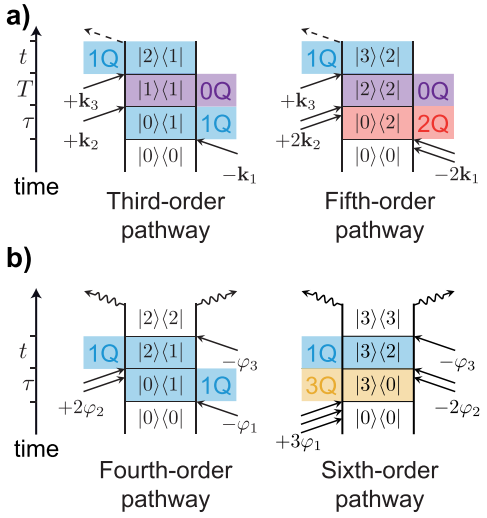

Figure 1. Description of nonlinear signals using double-sided Feynman diagrams. The different coherences are marked with the colors (0Q in purple, 1Q in blue, 2Q in red, and 3Q in yellow). (a) Examples of diagrams that contribute to coherently detected third-order 1Q0Q1Q (left) and fifth-order 2Q0Q1Q (right) signals. (b) Examples of diagrams that contribute to the action-detected fourth-order 1Q1Q signal (left) and the sixth-order 3Q1Q signal (right).

diagrams for a coherently detected experiment: on the left a third-order pathway contributing to a 1Q0Q1Q signal and on the right a pathway of a fifth-order signal corresponding to the 2Q0Q1Q signal. We mark each coherence with a specific color: 0Q in purple, 1Q in blue, and 2Q in red. In Figure 1b we show two diagrams connected to action-detected spectroscopy (where the 3Q coherence is marked in yellow). Instead of phase matching, in this example the signal is isolated via phase cycling, which is discussed below. In the diagrams, the wavevectors are replaced by the relative phases connected to the electric fields. An arrow pointing to the left is connected with $-\varphi$ while an arrow pointing to the right is connected with $+\varphi$. Figure 1b shows diagrams contributing to a fourth-order 1Q1Q signal and a sixth-order 3Q1Q signal. Both signals can be isolated in an action-detected three-pulse experiment as we will discuss later. The order of a process can be read out from the Feynman diagram by counting the number of interactions with the electric fields.

Let us now discriminate, from such multiquantum signals, the nonlinear orders that correspond to the different terms of the perturbative expansion. One might naively think that, for example, the coherently detected 1Q0Q1Q signal should correspond to a third-order signal. However, higher (than the third) nonlinear orders generally contribute as well. The influence of the higher-order signals on a specific signal can be controlled by the intensities of the pulses. For example, they are usually chosen in such a way that the 1Q0Q1Q signal is dominated by the third-order response, while higher-order terms do not contribute "significantly," where the level of tolerated contributions is often not specified or characterized quantitatively. If the intensity of the two pump pulses is increased, the 1Q0Q1Q signal will be substantially "contaminated" by higher-order signals, i.e., fifth- and higher-order signals. Higher-order signals can be characterized independently by isolating appropriate multiquantum signals. In other words, each multiquantum signal has a lowest-order contribution with lower-order signals not present. For example, in coherently detected 2D spectroscopy in the pump−probe geometry, the 2Q0Q1Q signal illustrated in Figure 1a is at least a fifth-order signal. Note that, in our convention, a coherently detected $XQYQZQ$ signal dominated by the $(2n+1)$th nonlinear order corresponds to the population-detected $XQYQZQ$ signal dominated by the $(2n+2)$th nonlinear order (n = 1, 2, 3,···), and they are both based on the same underlying generalized response function.[54] There is no general mapping from the X, Y, Z to the leading order response of a signal, as for example, it is also possible to acquire signals involving 2Q coherences that are lower than fifth order. For example, in so-called double-quantum spectroscopy, one measures a coherently detected third-order 1Q2Q1Q signal containing a 2Q coherence during the population time by choosing the phase-matching condition $+\mathbf{k}_1 + \mathbf{k}_2 - \mathbf{k}_3$,[6] and one can similarly apply phase cycling to extract a fourth-order 1Q2Q1Q signal in fluorescence-detected 2D spectroscopy.[59]

While certain multiquantum signals such as the mentioned 2Q0Q1Q signal might have no contribution of lower-order signals, i.e., the leading order is a higher-order term, in general, terms of even higher order are also present. The total contribution of contaminating higher-order terms can be kept low again by choosing an adequate intensity regime, i.e., using the intensity dependence of the different nonlinear order terms. The contamination by higher-order signals should be kept in mind and will be addressed explicitly in the section dealing with higher-order pump−probe spectroscopy. To simplify the discussion until then, we will mention only the leading order for each multiquantum signal, implying that the intensity regime was chosen such that the lowest nonlinear order of a certain multiquantum signal is the dominant term.

Let us now focus on the experimental approaches for obtaining higher-order signals. In this Perspective, we focus on two approaches, namely, selection by excitation frequency in coherently detected spectroscopy (Figure 2a) and selection via phase cycling in fluorescence-detected spectroscopy (Figure 2b). Other approaches such as phase-matching in fully noncollinear setups[6,60] as well as action-detected spectroscopy

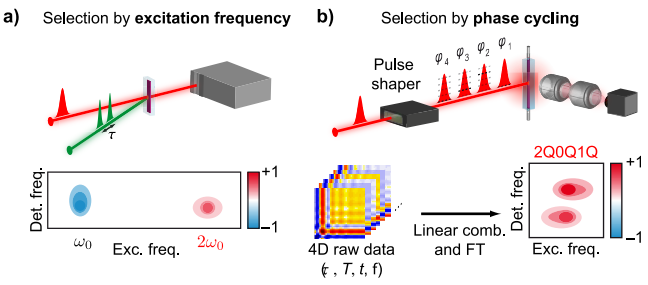

Figure 2. Overview of two experimental approaches discussed in this Perspective to isolate multiquantum signals predominantly corresponding to higher nonlinear orders in multidimensional spectroscopy. (a) In PP geometry, the first two (pump) pulses have the same wavevector. The higher-order signals are separated along the excitation frequency axis in the 2D spectrum because they oscillate at higher frequencies during time delay τ. (b) In action-based spectroscopy (here with fluorescence detection), the signal is measured using four pulses with variable time delays. The isolation of the signals is carried out by phase cycling. For phase cycling, the relative pulse phases are systematically varied by incrementing the absolute phases φ_i (i = 1, 2, 3, 4) of the second, third, and fourth pulses with respect to the first for each set of time delays.

https://doi.org/10.1021/acs.jpclett.3c01694
J. Phys. Chem. Lett. 2023, 14, 7556−7573

applying phase modulation[11,21,61−63] can also be used to isolate different signal contributions including higher-order signals.

In the PP geometry (Figure 2a) the two pump pulses, i.e., pulses 1 and 2, excite the system from the same direction, and the signal is emitted in the direction of the probe pulse, which also acts as the LO. Therefore, the purely absorptive spectrum, i.e., the sum of the rephasing and nonrephasing parts, can be measured directly. However, some fifth-order contributions, such as $-2\mathbf{k}_1 + 2\mathbf{k}_2 + \mathbf{k}_3$ and $+2\mathbf{k}_1 - 2\mathbf{k}_2 + \mathbf{k}_3$, are also emitted in the same direction as the third-order signals, because $\mathbf{k}_1 = \mathbf{k}_2$ in the PP geometry.[52,64] While these signals overlap spatially, we can separate them in the frequency domain along the excitation axis in the 2D spectrum.[64] The 2Q0Q1Q signal appears at around twice the central frequency ($2\omega_0$) of the excitation pulses and can be spectrally separated from the 1Q0Q1Q signal at ω_0. This can be directly inferred from the examples of double-sided Feynman diagrams for the two signals in Figure 1a. In the diagram contributing to the 1Q0Q1Q signal, a 1Q coherence is present during the coherence time τ (Figure 1a, left), while in the diagram for the 2Q0Q1Q signal, a 2Q coherence is present (Figure 1a, right). In order to discriminate such higher-order signals, the coherence time step size has to be chosen small enough according to the Nyquist theorem.[6] The first two pulses, i.e., the two pump pulses, can be created, for example, by a Mach−Zehnder interferometer or conveniently from one beam path by a pulse shaper or a common-path interferometer.[3,65] Polarization control in the PP geometry can be achieved with vector-field pulse shaping.[66,67] Another approach utilizes differently oriented polarizers for the probe pulse before and after the sample to suppress certain signal contributions.[68] In the PP geometry, rephasing and nonrephasing signal contributions are emitted in the same direction and can therefore not be separated spatially but can be separated via phase cyling[69] as described below in the context of action-based spectroscopy.

It is also possible to use incoherent observables to measure multidimensional spectra as shown in Figure 2b for the example of phase cycling using fluorescence detection.[12,59,70] Measurements using other incoherent observables such as photoelectrons,[15−17] ions,[18−20] and internal photocurrents[21−24] can be carried out as well. Note that these action-based approaches acquire a signal that is dependent on the excited-state population after the last light-pulse interaction, which means that a nonlinear signal of even order is measured (i.e., fourth order, sixth order, etc.). We analyzed the response functions for coherently detected and action-detected 2D spectroscopy, demonstrating their similarities and differences and derived a generalized response function for both techniques.[54] The excited-state population that is connected to the observable in fluorescence-detected 2D spectroscopy is created at the end of the sequence of pulses and can be influenced by dynamical processes such as EEA or internal conversion. Both effects can reduce the quantum yield of certain excitation pathways, resulting in their (partial) cancellation. The fundamental and practical differences of coherently and fluorescence-detected techniques were part of several recent studies.[9,27] Using fluorescence as an observable has the advantage that the solvent does not contribute to the signal because the solvent is usually not fluorescent, which makes fluorescence-detected methods well suited to track short-lived dynamics, with the potential to reach single-molecule sensitivity.[71]

In the scheme of Figure 2b, phase cycling is used for signal isolation. In phase cycling, the relative pulse phases are incremented in discrete, equidistant steps, enabling discrimination of desired signals from the undesired background. Similar to phase matching, phase cycling exploits the unique phase signatures of nonlinear signals for their discrimination. The concept of phase cycling was originally introduced in the context of 2D NMR spectroscopy to suppress unwanted artifacts.[72] Later, Tan developed a theory for phase cycling in optical 2D spectroscopy,[73] which was then adapted to 2D spectroscopy in the pump−probe geometry.[69] Depending on the desired nonlinear signals, the phase-cycling scheme must be chosen carefully, as we discuss further below. For multiquantum signals dominated by higher-order responses, phase-cycling schemes must employ smaller increments for the relative phases, analogously to coherently detected spectroscopy where smaller delay step sizes are needed to resolve multiquantum signals oscillating at higher frequencies.[59] Experimentally, phase cycling can be carried out using a pulse shaper. Note that if the time delays are controlled by a pulse shaper, the maximum available time delays are limited by the properties of the pulse shaper such as the crystal length in the case of an AOPDF, which results in a delay limit up to a few picoseconds.[74,59,75] The advantage of a single-beam geometry is that phase stability is inherently assured, which eliminates the need for employing an additional procedure to determine the absolute phase of the nonlinear signals. For each set of delays, the relative phases of the pulses are varied. The nonlinear signals therefore depend on the delays as well as on the relative phases of the pulses, analogous to the signals in noncollinear, coherently detected 2D spectroscopy that depend on the delays and on the distinct wavevectors.

Various nonlinear signals in fluorescence-detected 2D spectroscopy can then be constructed by weighting the phase- and delay-dependent raw data with phase-specific factors.[73] In addition to dealing with potential artifacts introduced by the pulse shaper, one has to prevent artifacts from potential nonlinearities of the detector either by calibration or by acquiring data only in the linear regime of the detector.[55] Spectral interferometry can be used to characterize all pulse sequences in 2D spectroscopy on the fly during an actual experiment, ensuring that artifacts are small and allowing the precise electric fields to be taken into account in simulations.[76]

Higher-Order Fluorescence-Detected 2D Spectroscopy. As a first application example, we now discuss how phase cycling in fluorescence-detected 2D spectroscopy can be used to separate nonlinear signals from each other. Let us consider a three-pulse excitation sequence. The total phase of the signal, φ_{tot}, can be decomposed into

$$\varphi_{tot} = \alpha\varphi_1 + \beta\varphi_2 + \gamma\varphi_3 \quad (1)$$

with the phases φ_i (i = 1, 2, 3) of the three pulses corresponding to the zeroth-order coefficients of a Taylor expansion of spectral phase. Note that interactions with $+\varphi_i$ as well as $-\varphi_i$ are possible, since these are associated with the positive and negative frequencies that are both contained in the real-valued electric field. The set of the three coefficients α, β, and γ, each of which is an integer, corresponds to the interaction pattern with pulses 1 to 3. Each coefficient represents the number of electric-field interactions with $+\varphi_i$ minus the number of interactions with $-\varphi_i$ that occur with the corresponding pulse i. In the rotating-wave approximation, an

https://doi.org/10.1021/acs.jpclett.3c01694
J. Phys. Chem. Lett. 2023, 14, 7556−7573

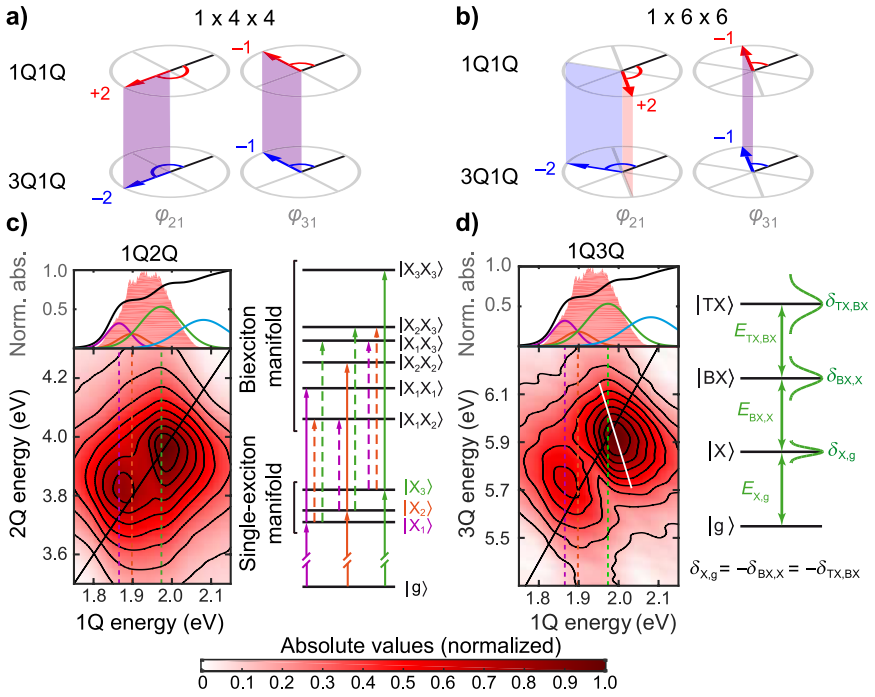

Figure 3. Multidimensional spectroscopy using fluorescence detection combined with phase cycling. (a, b) The isolation of two signal contributions via phase cycling is illustrated by plotting the signal-specific weighting factors as vectors in the φ_{21} space and φ_{31} space. We show the vectors for the phase combinations of the 1Q1Q signal (top) and the 3Q1Q signal (bottom). For a $1 \times 4 \times 4$ phase-cycling scheme (a), the vectors corresponding to specific signals point in the same direction (i.e., the signals are aliased). For a $1 \times 6 \times 6$ phase-cycling scheme (b), the vectors are separated in φ_{21} space allowing one to isolate the 1Q1Q and the 3Q1Q spectrum without aliasing. (c) 1Q2Q spectrum (absolute magnitude, normalized) of $CdSe_{1-x}S_x/ZnS$ quantum dots in toluene. The absorption spectrum (black line) as well as the pump spectrum (red shaded area) are shown on top of the 2D spectrum. The transitions of the three excitons that are predominately excited are shown as vertical dashed lines. The resulting 2D spectrum displays the projection of several biexciton states (see energy-level scheme on the right) to the exciton states. (d) 1Q3Q spectrum (absolute magnitude, normalized) of the same sample extracted from the same experiment. The observed peak tilt (white line) is a result of correlated transition energy fluctuations (δ) between ground (g), exciton (X), biexciton (BX), and triexciton (TX) states. Panels c and d are reprinted with permission from ref 78. Copyright 2021 American Chemical Society.

interaction with $+\varphi_i$ corresponds to an excitation of the ket side or a de-excitation of the bra side, while an interaction with $-\varphi_i$ corresponds to an excitation of the bra side or a de-excitation of the ket side of the density matrix. Since we are observing fluorescence, the final state after the interaction with the last pulse must be a population in an excited state, i.e., a diagonal element of the density matrix. A population can only be generated by the last pulse when the condition

$$\alpha + \beta + \gamma = 0 \tag{2}$$

is fulfilled.[73] If the pulse intensities are chosen so that the highest order of nonlinearity that needs to be considered is R, a limit on the absolute number of total interactions is provided

$$|\alpha| + |\beta| + |\gamma| \leq R \tag{3}$$

While the coefficients can be negative, the observed order of nonlinearity depends only on the number of interactions. From eq 2 it follows that the coefficients are not independent of each other. We can hence reference the phases to the phase of the first pulse, resulting in $\varphi_{21} \equiv \varphi_2 - \varphi_1$ and $\varphi_{31} \equiv \varphi_3 - \varphi_1$.

The raw data, $p(\tau, t, \varphi_{21}, \varphi_{31})$, depend on the time delay τ between pulses 1 and 2, the delay t between pulses 2 and 3, and the relative phases of the pulses, φ_{21} and φ_{31}. The discrete 2D Fourier transformation of $p(\tau, t, \varphi_{21}, \varphi_{31})$ with respect to φ_{21} and φ_{31} gives the various nonlinear signal contributions $\tilde{p}$ as[73]

$$\tilde{p}(\tau, t, \beta, \gamma) = \frac{1}{LM} \sum_{l=0}^{L-1} \sum_{m=0}^{M-1} p(\tau, t, l\Delta\varphi_{21}, m\Delta\varphi_{31}) \, e^{-i\beta l\Delta\varphi_{21}} e^{-i\gamma m\Delta\varphi_{31}} \tag{4}$$

with the total number of phase-cycling steps L in φ_{21} space and M in φ_{31} space and associated phase increments $\Delta\varphi_{21} = 2\pi/L$ and $\Delta\varphi_{31} = 2\pi/M$. Note that the nonlinear signal contributions do not depend on α because we used relative phases. We can label a phase-cycling scheme by the number of experimental steps L and M as a "$1 \times L \times M$" phase-cycling scheme where the first number reflects the fact that the relative phases are referenced to pulse 1 and thus the phase of pulse 1 is not cycled. Each signal contribution is characterized by its interaction pattern, which is reflected by the values of coefficients β and γ. The different multiquantum signals can thus be retrieved from one set of raw data with eq 4 by inserting signal-specific values for β and γ.

Phase-cycling schemes must have an appropriate number of steps to discriminate between various multiquantum signals. To illustrate this, let us discuss a three-pulse sequence with the goal to separate a fourth-order multiquantum signal from another sixth-order multiquantum signal. In order to visualize the ability of a particular phase-cycling scheme to separate different signal contributions, we can sketch the φ_{21} and φ_{31} spaces in polar coordinates, as in Figure 3a. The number of phase-cycling steps L and M divides the unit circle into equally sized sections. We can then plot the signal-specific phase

https://doi.org/10.1021/acs.jpclett.3c01694
J. Phys. Chem. Lett. 2023, 14, 7556−7573

vectors of $e^{-i\beta\Delta\varphi_{21}}$ and $e^{-i\gamma\Delta\varphi_{31}}$ in the φ_{21} and φ_{31} space, respectively. In Figure 3a, we show the values of β and γ next to the corresponding vectors. As an example, we show the vectors for the fourth-order 1Q1Q signal, which corresponds to the correlation of 1Q coherences during τ and t, and the 3Q1Q signal, which corresponds to a sixth-order signal with a three-quantum (3Q) coherence during τ and a 1Q coherence during t. To distinguish the two signals via phase cycling, the vectors must differ either in the φ_{21} space or in the φ_{31} space (or in both). For a $1 \times 4 \times 4$ phase-cycling scheme (Figure 3a), we can see that both vectors for $\beta = -2$ and $\beta = +2$ in the φ_{21} space as well as the vectors in the φ_{31} space are the same ($\gamma = -1$) for the two different signals. The specific values of β and γ can be determined by inspection of the double-sided Feynman diagrams describing the signals (Figure 1b). The $1 \times 4 \times 4$ phase-cycling scheme is thus not sufficient to distinguish the 1Q1Q signal from the 3Q1Q signal; both the fourth- and sixth-order signals contribute to the same $\tilde{p}$ in eq 4. This can be easily seen in Figure 3a where the red and blue vectors in the scheme point in the same direction. Hence, the two multiquantum signals are mixed, and we say that these signals are "aliased". In the example, an attempt to extract the 1Q1Q signal using eq 4 yields contributions from the 3Q1Q signal. For a higher phase-cycling scheme, i.e., smaller phase increment steps, the two vectors point in different directions (Figure 3b, for $1 \times 6 \times 6$), resolving the coefficient ambiguity.[55] Note that a $1 \times 5 \times 5$ phase-cycling scheme would be insufficient to discriminate all multiquantum signals up to sixth order. In general, an appropriate phase-cycling scheme ensures the separation of multiquantum signals from each other up to a certain order, under the assumption that higher orders do not contribute. The appearance of a multiquantum signal that is predominantly of sixth order implies that the pulse intensities are large enough that there will also be sixth-order contaminations of the multiquantum signals that are predominantly of fourth order. Note that eighth-, tenth-, or even higher-order signals can additionally contribute, and the intensity regime needs to be chosen appropriately to keep the contaminations small, or one needs to isolate these higher orders as we discuss in Higher-Order Pump−Probe Spectroscopy.

The power of fluorescence-detected higher-order 2D spectroscopy using phase cycling is that many 2D spectra can be extracted from the same data set.[59,77] Each extracted 2D spectrum shows correlations among various coherences. The phase-cycling protocol can be directly extended to specific multiquantum signals by choosing a higher-order phase-cycling scheme. Furthermore, instead of a three-pulse sequence, multipulse sequences with an increasing number of pulses (and thus higher dimensions) could be applied, which would allow us to systematically investigate correlations between more than three coherences.

We illustrate the capabilities of phase cycling on the example of quantum dots measured with a $1 \times 6 \times 6$ (36-fold) phase-cycling scheme in the experimental configuration of Figure 2b.[78] We have shown that for a 36-fold phase-cycling scheme, six predominantly sixth-order multiquantum signals, and three signals that are dominated by fourth order, can be isolated.[55] In Figure 3c, we show the absolute magnitude of the 1Q2Q spectrum (predominantly a fourth-order signal) of $CdSe_{1-x}S_x$/ZnS alloyed core/shell quantum dots. The first three excitons were excited with a broadband pulse (Figure 3c, top). The 1Q2Q spectrum correlates the transition from the ground state to the single-exciton manifold with the transitions from the ground state to the biexciton manifold. Due to the broadband excitation, six biexciton states were excited (Figure 3c, right). Especially the biexciton states that are energetically higher than the lowest biexciton state cannot be directly probed with other methods such as time-resolved photoluminescence. With the help of simulations, the binding energies of all the six involved biexciton states as well as their transition dipole moments (shown as vertical arrows in Figure 3c, where the dashed arrows correspond to somewhat lower transition dipole moments) could be determined.

While the 1Q2Q signal is dominantly of fourth order, the utilized phase-cycling scheme provided the opportunity to extract several other multiquantum signals as higher-order contributions. One of these contributions is the 1Q3Q spectrum (Figure 3d), which is dominated by the sixth order. For the quantum dot sample, this spectrum provides information about the transition energy fluctuations. We find strong anticorrelation between the ground-state to single-exciton transition energy fluctuation with bandwidth $\delta_{X,g}$ and the single-exciton to biexciton transition energy fluctuation with bandwidth $\delta_{BX,X}$ as well as anticorrelations between the ground-state to single-exciton transition energy fluctuation and the biexciton to triexciton transition energy fluctuation with bandwidth $\delta_{TX,BX}$. In other words, the amplitude of the transition energy fluctuation of the single-exciton state determines whether the biexciton and triexciton states undergo stabilization, i.e., a shift to higher binding energies, or destabilization, i.e., a shift to lower binding energies.

Moving from three-pulse to four-pulse sequences allows one to measure dynamics over the additional delay T. We used a four-pulse sequence to investigate the electronic structure of a dianion with interesting photophysical properties such as high fluorescence quantum yield.[59] We combined shot-to-shot pulse shaping with a 1 kHz amplified laser system. This measurement procedure allowed us to stream the full $1 \times 5 \times 5 \times 5$ phase-cycling scheme with all time delays, i.e., a total of 421875 sequences, in just 8 min (without averaging). The employed higher phase-cycling schemes isolated 15 different spectra, 3 dominantly of fourth order and 12 dominantly of sixth order, allowing us to map the energetic landscape up to triply excited states and decipher their energies, dynamics, and vibrational displacement.[59] Another example demonstrated the use of a so-called cogwheel phase-cycling scheme, which may reduce the number of total phase steps in some cases. This scheme was used to measure the 2Q2Q signal (the 2Q photon echo) of a dimer and a squaraine polymer, in predominantly eighth order of nonlinearity, with which one can access their respective biexciton lineshapes.[79]

Coherently Detected Higher-Order 2D Spectroscopy. Coherently detected higher-order 2D spectroscopy in the PP geometry (Figure 2a) allows one to isolate a 2Q0Q1Q signal with a parametric dependence on T. We now discuss how this 2Q0Q1Q signal can be used to track exciton diffusion. The 2Q0Q1Q signal is dominated by two-fifth-order signals with phase-matching conditions of $-2\mathbf{k}_1 + 2\mathbf{k}_2 + \mathbf{k}_3$ and $+2\mathbf{k}_1 - 2\mathbf{k}_2 + \mathbf{k}_3$. In excitonic systems, the dynamics of the biexciton population can be measured by tracking the 2Q0Q1Q signal over the time delay T between the two pump pulses and the probe pulse. What can we learn from biexciton dynamics? In extended systems, i.e., large excitonic systems consisting of many coupled subunits (molecular aggregates, polymers, photosynthetic membranes, etc.), the spectral signature of

https://doi.org/10.1021/acs.jpclett.3c01694
J. Phys. Chem. Lett. 2023, 14, 7556−7573

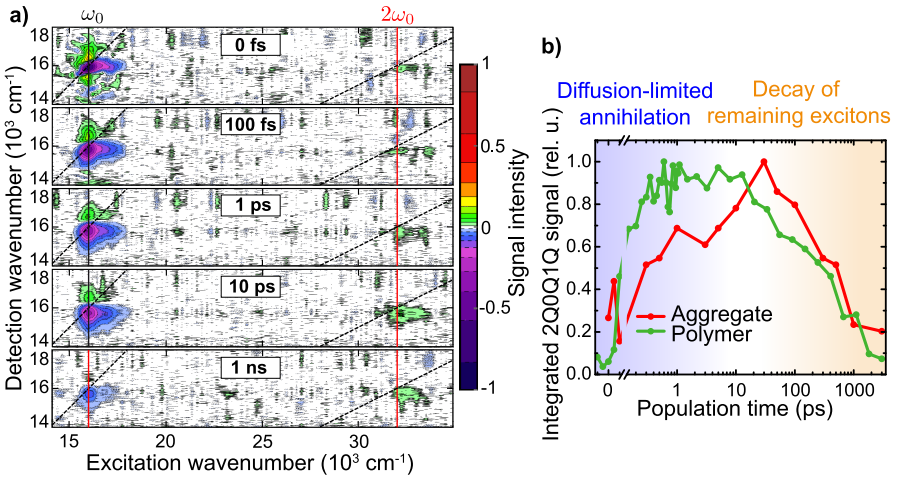

Figure 4. Coherently detected 2Q0Q1Q signals using 2D spectroscopy in PP geometry. (a) The 2D spectrum of a perylene bisimide-based J-aggregate exhibits two distinct features: a predominantly negative signal at ω_0 and a positive signal at $2\omega_0$. (b) The population time evolution of the integrated 2Q0Q1Q signal of extended systems is dominated by EEA. We show two examples of such systems: a supramolecular J-aggregate (red) and a squaraine polymer (green). The 2Q0Q1Q signals show a rise due to diffusion-limited annihilation (blue-shaded region), followed by a decay according to the exciton lifetime (orange-shaded region). Both transients are normalized to their individual maxima. The data of the squaraine polymer were measured under similar conditions as in our previous publication[82] but with more population time steps. Panel a is adapted with permission from ref 64.

excitons is not affected by propagation if their local environment is the same everywhere on average. However, we can exploit additional processes that occur when two excitons come spatially close together. This can lead to the annihilation of one of the two excitons, i.e., EEA. In an extended system, where the two excitons are on average not close to each other directly after excitation, a period of exciton transport must occur before the annihilation takes place. The coherently detected 2Q0Q1Q signal in extended excitonic systems is dominated by EEA, and thus the dynamics of exciton transport are reflected by a rise of the 2Q0Q1Q signal with time.[64] In other words, the annihilation acts as a "probe" for exciton transport in extended systems, which is well-known from intensity-dependent transient absorption studies where third- and fifth-order contributions are mixed together, i.e., biexciton dynamics including EEA mixes into the single-exciton dynamics as outlined in the introduction.[43−45,80] However, if we obtain a 2Q0Q1Q signal instead, we can obtain direct access to the annihilation dynamics.[81] While for extended systems such as polymers it was shown theoretically that the frequency-integrated 2Q0Q1Q signal is dominated by the dynamics of the biexciton states, i.e., EEA,[82,83] in general also single-exciton dynamics as well as ground-state dynamics can contribute to the 2Q0Q1Q signal.[54,84,85] As shown recently in the example of quantum dots,[85] this fact can be used to get additional information about the transition dipole moments.

As an example, we show in Figure 4a the coherently detected 2D spectrum of a perylene bisimide-based J-aggregate, acquired in PP geometry.[64] The signal at around ω_0 on the excitation axis is dominated by a negative contribution (blue-violet) that decays over the population time with a single-exciton lifetime. Note that in our convention, third-order ground-state bleach and stimulated emission are plotted as negative signals in accordance with the convention of transient absorption where ground-state bleach corresponds to reduced absorption. In contrast to the signal at ω_0, the 2Q0Q1Q signal that is predominantly of fifth order at $2\omega_0$ on the excitation axis has a positive sign and rises with the population time.[6] The integrated 2Q0Q1Q signal of extended systems probes the biexciton dynamics, which are dominated by EEA as shown in Figure 4b (red curve). After excitation, the two excitons must be close to each other in order to annihilate. The kinetics of the transport process is responsible for the slow rise of the 2Q0Q1Q signal at early times (Figure 4b, blue-shaded region). After reaching a plateau, the remaining excitons decay according to the exciton lifetime (Figure 4b, orange-shaded region). In Figure 4b we also show, for comparison, the integrated 2Q0Q1Q signal of a squaraine copolymer made on average from 18 dimer units (green curve). This polymer, which is also an extended system made from repeating subunits, differs, however, in its electronic structure from the molecular J-aggregate due to the covalently bound subunits. While the decay of the 2Q0Q1Q signal is similar in both systems because of their comparable exciton lifetimes, the rise of the 2Q0Q1Q signals differs significantly, reflecting the faster annihilation in the polymers compared with the J-aggregates. The diffusion coefficient as well as the exciton delocalization length can be obtained by modeling the fifth-order signal dynamics.[64]

Furthermore, the 2Q0Q1Q signal can be used to study the "character" of exciton diffusion. We used the 2Q0Q1Q signal to model exciton diffusion in a series of squaraine copolymers that differ in their average length.[82] Interestingly, we found that the often-applied assumption of normal diffusion[86,87] does not hold in these polymers and that exciton motion can be better described by subdiffusive behavior. A reason for such anomalous diffusion could be the energetically disordered structure of the polymers. We also used coherently detected 2Q0Q1Q spectroscopy to investigate the exciton dynamics in double-walled tubular aggregates.[88] There, we measured the interplay between exciton transport and diffusion within each of the tubes. Additional information about the geometrical and energetic disorder of a system can be obtained by analysis of the anisotropy of the 2Q0Q1Q signal.[83] Furthermore, analysis of the peak shape reveals information about the correlation of fluctuations between states[89] similar to the case of

https://doi.org/10.1021/acs.jpclett.3c01694
J. Phys. Chem. Lett. 2023, 14, 7556−7573

Table 1. Example Multiquantum Signals with Their Leading Nonlinear Order as Well as Detection Scheme and Application

Leading order	$XQYQZQ/XQZQ$	Detection scheme	Application	Reference
5	2Q0Q1Q	$\mp 2\mathbf{k}_1 \pm 2\mathbf{k}_2 + \mathbf{k}_3$ (PP geometry)	Exciton−exciton annihilation, exciton diffusion	64, 82, 88, 90
7	3Q0Q1Q	$\mp 3\mathbf{k}_1 \pm 3\mathbf{k}_2 + \mathbf{k}_3$ (PP geometry)	Multiexciton annihilation	58
6	3Q1Q, 1Q3Q	36-fold (1 × 6 × 6) phase cycling	Multiexciton binding energies, multiexciton correlation, triply excited molecular states	91, 78
6	2Q0Q1Q, 1Q0Q2Q	125-fold (1 × 5 × 5 × 5) phase cycling	Exciton−exciton annihilation	90
6	2Q0Q1Q	125-fold (1 × 5 × 5 × 5) phase cycling	Properties of doubly excited states	59
8	2Q2Q	33-fold cogwheel phase cycling	Biexciton homogeneous line width	79

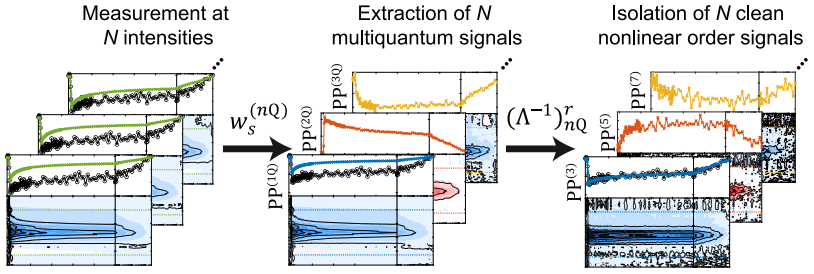

Figure 5. Higher-order PP spectroscopy. A set of N PP spectra is measured in which the excitation intensity is systematically varied (left). A linear combination of the intensity-dependent measurements, weighted with $w_s^{(nQ)}$, is used to extract N multiquantum signals (middle). Correction of the contaminations from various overlapping nonlinear orders using the matrix $(\Lambda^{-1})^r_{nQ}$ leads to N clean nonlinear-order signals (right). The so-obtained third-order signal (blue curve on the right panel) agrees with the low-power measurement used as a reference (black data points), demonstrating that the obtained third-order signal is free of higher-order contributions. Adapted with permission from ref 85. Copyright 2023.

fluorescence-detected higher-order spectroscopy in Figure 3d.[78]

The examples provided above demonstrate that fifth-order 2D spectroscopy is well-suited to tracking exciton diffusion in extended systems. Compared to low-order techniques, the fifth-order signal is measured directly without third-order signals contributing to the signal, resulting in direct access to EEA in the case of extended excitonic systems. The separate measurement of the biexciton dynamics, including EEA, simplifies the analysis. This separation is an advantage compared to previous studies utilizing variations of the excitation intensity where third- and fifth-order signals are mixed together.[43−45]

Let us now briefly compare fluorescence-detected and coherently detected 2D spectroscopy. In coherently detected 2D spectroscopy, the 2Q0Q1Q signal can be very well used to track EEA.[60,64,82] The 2Q0Q1Q signal can be isolated easily by its specific excitation frequency without the need for phase cycling. In fluorescence-detected 2DES, EEA is reflected in the cross-peak amplitude already in the fourth-order signal.[27] The higher-order signals, isolated by phase cycling or phase modulation, include single-exciton dynamics as well, and additional steps have to be taken to isolate EEA.[54,60] On the other hand, an advantage of fluorescence-detected spectroscopy and other action-detected variants is that they are background-free, which allows one to avoid strong coherent artifacts. This is especially suitable for signals close to $T = 0$. Because a single excitation beam can be used, fluorescence-detected 2D spectroscopy is highly suited to be combined with spatially resolved methods, which will be discussed at the end of this Perspective. We summarize several of the experiments discussed in this Perspective with the (dominating) nonlinear order, multiquantum signal, detection scheme, and application in Table 1. There are many more examples of high-order spectroscopies, several of which are mentioned throughout this Perspective.[46−53,60,62,84,89]

Higher-Order Pump−Probe Spectroscopy. So far, we discussed multidimensional methods to probe multiquantum signals. The technique of PP (transient absorption) spectroscopy is closely related to multidimensional spectroscopy, as outlined in the introduction. Using the close relation between the two techniques, we developed a technique to *isolate* nonlinear signals of a particular order in a PP experiment. In contrast to the previously discussed multiquantum signals, which have been dominated by a particular nonlinear order (but are contaminated with higher orders in general), we can obtain signals representing "clean" nonlinear orders, i.e., free of contamination by higher nonlinear orders, using the PP approach. The complete procedure is discussed in detail below, and Figure 5 illustrates an example with squaraine polymers. The key idea is to use PP measurements at specific excitation intensities (Figure 5, left). From these, several multiquantum signals can be extracted via linear combinations determined with a set of weight factors $w_s^{(nQ)}$ (Figure 5, middle). These multiquantum signals still contain overlapping contributions of nonlinear signals from various nonlinear orders. In a next step, the multiquantum signals are used to construct PP signals of clean nonlinear order using the matrix $(\Lambda^{-1})^r_{nQ}$ (Figure 5, right).

Let us now discuss the procedure shown in Figure 5 in more detail. We begin by comparing a PP experiment to coherently detected 2D experiments in PP geometry. The full 2D experiment has much more information, but the EEA kinetics, as in Figure 4b, are determined by keeping only the excitation frequency $2\omega_0$ and integrating the 2Q0Q1Q signal over the detection and excitation frequency; i.e., information such as the line shapes along the excitation and detection axes is not evaluated. This integration gives a signal equivalent to the

https://doi.org/10.1021/acs.jpclett.3c01694
J. Phys. Chem. Lett. 2023, 14, 7556−7573

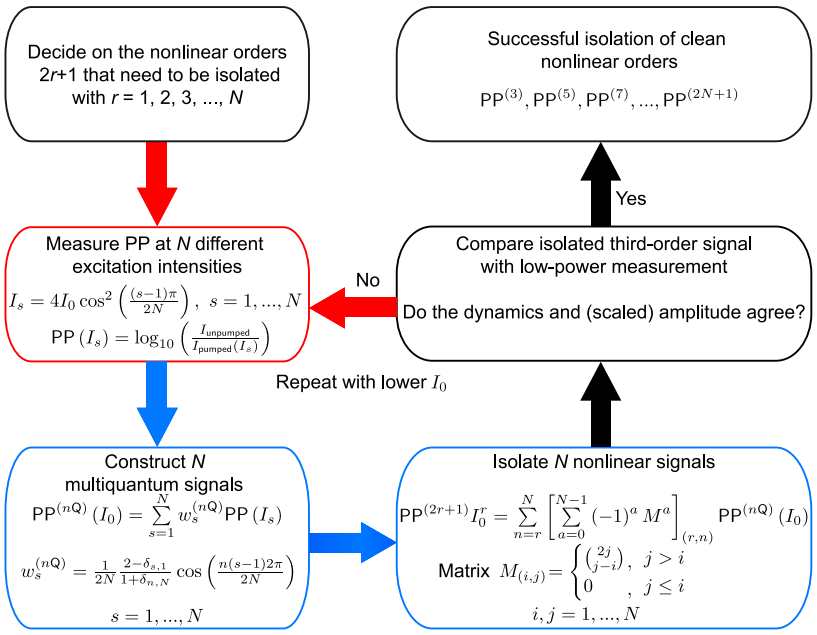

Figure 6. Higher-order PP spectroscopy. Measurements are depicted in red, data analysis is in blue, and validation is in black. The different nonlinear orders are isolated by using linear combinations of measurements at different excitation intensities I_s. Comparing the extracted third-order signal with a low-power measurement reveals if the chosen intensity I_0 with the particular numbers of intensities N is enough to extract all the present nonlinear orders.[85]

frequency-integrated PP signal. The 2Q0Q1Q signal with phase-matching condition $\pm 2\mathbf{k}_1 \mp 2\mathbf{k}_2 + \mathbf{k}_3$ is emitted in the same direction as the probe pulse itself (because $\mathbf{k}_1 = \mathbf{k}_2$) but occurs at $2\omega_0$ along the excitation frequency axis in the 2D spectrum. The excitation axis of the 2D spectrum is only needed to separate the different multiquantum contributions that are emitted in the same spatial direction. Integrating a 2D spectrum over all excitation frequencies corresponds to simply measuring at $\tau = 0$, i.e., a PP signal. For integration over the whole excitation frequency axis, the result would be the normal PP spectrum according to the projection-slice theorem,[6,92] with all the multiquantum signals added up, and the unique 2Q0Q1Q signature would be lost.

It is still possible to separate the (integrated) multiquantum signals from multidimensional spectroscopy, however, even when measuring a PP spectrum with $\tau = 0$. For this purpose, we take inspiration from phase cycling. While we had introduced phase cycling for action-based detection (Figure 2b) as illustrated in the fluorescence-detected 2D experiments on quantum dots (Figure 3), it is also possible to implement phase-cycling protocols for coherently detected 2D spectroscopy such as in PP geometry. Viewing the single pump pulse in PP spectroscopy as two pulses with zero time delay in 2D spectroscopy, phase cycling reduces to a mere variation of intensity, because the two coincident pulses interfere constructively or destructively, depending on their relative phase. To illustrate this, consider the equation for a collinear double pulse with the delay τ in phase cycling

$$E_{\text{pump}}(t) = e^{-i\omega_0 t + i\mathbf{k}_{\text{pump}}\cdot\mathbf{r}}\left(\underbrace{E_0(t)}_{\text{pulse 1}} + \underbrace{E_0(t+\tau)e^{-i\omega_0\tau + i\phi_s}}_{\text{pulse 2}}\right) + \text{c.c.} \tag{6}$$

where c.c. is the complex conjugate of the previous term, $E_0(t)$ is the complex envelope of the electric field (including chirp), ω_0 denotes the central frequency, $\mathbf{k}_{\text{pump}}$ is the common wavevector of both pulses, $\mathbf{r}$ is the position (which is integrated out when taking into account phase matching during propagation through the sample), and ϕ_s is the relative phase between both pulses.[85] Evaluated at $\tau = 0$ and inserting phase-cycling steps for ϕ_s, eq 6 leads to a mere intensity variation

$$I_s = 4I_0 \cos^2\left(\frac{(s-1)\pi}{2N}\right), \quad s = 1, \ldots, N \tag{7}$$

with the "base" intensity I_0 and N "intensity-cycling" steps with index s. The maximum intensity of $4I_0$ in an experiment is obtained by setting $s = 1$. For other values of s, the excitation intensity is effectively reduced. For example, for $N = 3$, intensities of $4I_0$, $3I_0$, and I_0 emerge from eq 7. Just as phase cycling allows extracting the multiquantum signals in a 2D experiment, applying intensity cycling to PP spectroscopy produces multiquantum signals without requiring 2D data. Here, we focus on intensity variation of the excitation pulses only, while the probe pulse is considered weak. Therefore, each multiquantum signal has the form nQ0Q1Q, and for shorthand notation we will drop the 0Q and 1Q and simply define multiquantum signals as nQ signals. Note that we define the multiquantum signals in PP spectroscopy as nQ signals although multiple-quantum coherences are actually not probed. We keep the notation in order to stress the close connection between PP and 2D spectroscopy, i.e., the PP signals correspond to the multiquantum signals probed via 2D spectroscopy for $\tau = 0$.

As an example, we start by measuring the PP signal for the N excitation intensities given by eq 7, as shown in Figure 6 (left, red box). The different nQ signals, $\text{PP}^{(n\text{Q})}$, are then isolated by suitable linear combinations of the raw data, adding the measurements $\text{PP}(I_s)$ at different excitation intensities I_s with different weights (Figure 6, blue box in the lower left corner)

https://doi.org/10.1021/acs.jpclett.3c01694
J. Phys. Chem. Lett. 2023, 14, 7556−7573

$$\mathrm{PP}^{(n\mathrm{Q})}(I_0) = \sum_{s=1}^{N} w_s^{(n\mathrm{Q})} \mathrm{PP}(I_s) \tag{8}$$

where the weights

$$w_s^{(n\mathrm{Q})} = \frac{1}{2N} \frac{2 - \delta_{s,1}}{1 + \delta_{n,N}} \cos\left(\frac{n(s-1)2\pi}{2N}\right), \quad s = 1, \ldots, N \tag{9}$$

are given by the phase-cycling rules,[73] but now adapted to the PP case.[58,85]

For weak excitation intensities, $\mathrm{PP}^{(1\mathrm{Q})}$ is dominated by a third-order nonlinear signal. For higher excitation intensities, a fifth-order signal also contributes. The fifth-order signal is present at two positions: first, as a 2Q signal and second, as a fifth-order contamination to the 1Q signal. If the excitation intensity is increased even further, seventh-order contributions can no longer be neglected, and they appear at the 3Q signal and as contaminations of both the 2Q and 1Q signals.

The uncontrolled mixing of nonlinear orders is a general problem in femtosecond spectroscopy, independent of the type of measured system. At low excitation intensity, one can suppress contamination from higher-order signals but must accept a correspondingly low SNR, whereas at high excitation intensity, one can achieve an improved SNR but must deal with contamination from higher orders. We offer a solution to this long-standing problem[93,94] by utilizing the multiquantum signals $\mathrm{PP}^{(n\mathrm{Q})}$ to obtain the clean nonlinear order contributions, i.e., by separating the different parts of perturbative expansion. In order to extract clean nonlinear orders from PP experiments, we must know quantitatively how much each particular nonlinear order contributes to each nQ signal. We here concentrate on the odd orders seen in coherent detection such as in PP spectroscopy. The coefficients for the contaminations by various nonlinear orders of an nQ signal can be found in two ways. We can either perform an analysis of the double-sided Feynman diagrams[58] or work directly with the phase-cycling structure.[85] In general, the $(2n + 1)$th-order nonlinear PP signal scales with the excitation intensity to the power n, e.g., linear in intensity for a third-order signal. This scaling is the reason why researchers trying to avoid contaminations from higher orders often state that their experiments were carried out in the "linear regime," despite the fact that a third-order response was measured.[6,95]

We now show how to remove artifacts, even when outside of the linear regime. This correction is possible using a matrix $(\Lambda^{-1})^r_{n\mathrm{Q}}$ that contains suitable correction factors connecting the clean nonlinear signals $\mathrm{PP}^{(2r+1)}$ with the experimentally extracted (contaminated) multiquantum signals $\mathrm{PP}^{(n\mathrm{Q})}$[58,85]

$$\begin{pmatrix} \mathrm{PP}^{(3)}I_0 \\ \mathrm{PP}^{(5)}I_0^2 \\ \mathrm{PP}^{(7)}I_0^3 \\ \mathrm{PP}^{(9)}I_0^4 \\ \mathrm{PP}^{(11)}I_0^5 \\ \mathrm{PP}^{(13)}I_0^6 \\ \vdots \end{pmatrix} = \begin{pmatrix} 1 & -4 & 9 & -16 & 25 & -36 & \ldots \\ 0 & 1 & -6 & 20 & -50 & 105 & \ldots \\ 0 & 0 & 1 & -8 & 35 & -112 & \ldots \\ 0 & 0 & 0 & 1 & -10 & 54 & \ldots \\ 0 & 0 & 0 & 0 & 1 & -12 & \ldots \\ 0 & 0 & 0 & 0 & 0 & 1 & \ldots \\ \vdots & \vdots & \vdots & \vdots & \vdots & \vdots & \ddots \end{pmatrix} \begin{pmatrix} \mathrm{PP}^{(1\mathrm{Q})}(I_0) \\ \mathrm{PP}^{(2\mathrm{Q})}(I_0) \\ \mathrm{PP}^{(3\mathrm{Q})}(I_0) \\ \mathrm{PP}^{(4\mathrm{Q})}(I_0) \\ \mathrm{PP}^{(5\mathrm{Q})}(I_0) \\ \mathrm{PP}^{(6\mathrm{Q})}(I_0) \\ \vdots \end{pmatrix} \tag{10}$$

The complete procedure is illustrated in Figure 6. At first, the experimenter has to decide on the highest nonlinear order that needs to be isolated (Figure 6, black box, top left), leading to a certain number of PP measurements at intensities given by eq 7 (Figure 6, red box). In a typical PP experiment, the spectral intensity of the probe beam $I_{\mathrm{pumped}}(I_s)$ with the pump beam present and I_{unpumped} without the pump beam present are detected via a spectrometer, resulting in the PP signal as a change of absorption for different pump intensities I_s. From these measurements, the nQ signals and further the clean nonlinear orders are constructed (Figure 6, blue boxes). Comparing the extracted third-order signal dynamics and amplitude to a scaled reference signal (as described below) is one way to ensure that the base intensity I_0 was chosen correctly, i.e., that the number of intensity-cycling steps is sufficient to extract all nonlinear orders that contribute (Figure 6, black box, right middle). Another option, not shown in Figure 6, is to directly assess the convergence of the recovered perturbation expansion, where each perturbation term is given by $\mathrm{PP}^{(2r+1)}$ in eq 11, by ensuring that the highest extracted order vanishes in the noise. If the reference signal and the extracted third-order signal disagree or the highest-order signal is not vanishing, then the intensity-cycling protocol has to be repeated with a lower value of I_0 or with larger N to take into account even higher orders.

We can also formally combine all of the steps, starting with the measurements at$N$ excitation intensities, separation of the multiquantum signals, and finally obtaining clean nonlinear signals, into one equation

$$\mathrm{PP}^{(2r+1)}I_0^r = \sum_{n=r}^{N} \left[\sum_{a=0}^{N-1} (-1)^a M^a\right]_{(r,n)} \sum_{s=1}^{N} \frac{1}{2N} \frac{2 - \delta_{s,1}}{1 + \delta_{n,N}} \cos\left(\frac{n(s-1)2\pi}{2N}\right) \mathrm{PP}\left[4I_0 \cos^2\left(\frac{s-1}{2N}\pi\right)\right] \tag{11}$$

where the inverse matrix $(\Lambda^{-1})^r_{n\mathrm{Q}}$ from eq 10 is expressed using the matrix M with matrix elements defined as

$$M_{(i,j)} = \begin{cases} \binom{2j}{j-i}, & j > i \\ 0, & j \le i \end{cases} \tag{12}$$

where $i = 1, \ldots, N$ is the index of the rows and $j = 1, \ldots, N$ the index of the columns. The matrix element $M_{(i,j)}$ quantifies the contribution of $(2j+1)$-th order response to the iQ signal, without the diagonal unity elements: $M = \Lambda - \mathbb{I}$ where $\mathbb{I}$ is the identity matrix. While eq 11 may look complicated at first sight, it is actually straightforward to implement and does not require any specialized software nor is the data acquisition complicated, making the procedure easy to carry out in any ultrafast spectroscopy laboratory.

After this general explanation, we now illustrate higher-order PP spectroscopy in the case of $N = 3$. Using the three different intensities of $4I_0$, $3I_0$, and I_0, the third-, fifth-, and seventh-order signals can be isolated. We select I_0 such that no signal higher than seventh order contributes significantly, which can be ensured as outlined above.

https://doi.org/10.1021/acs.jpclett.3c01694
J. Phys. Chem. Lett. 2023, 14, 7556−7573

In a first step of evaluation, we extract the 1Q signal, following eqs 8 and 9 and setting $n = 1$, as a linear combination from the measured PP data at the three excitation intensities

$$\mathrm{PP}^{(1Q)} = \frac{1}{6}[\mathrm{PP}(4I_0) + \mathrm{PP}(3I_0) - \mathrm{PP}(I_0)] \tag{13}$$

Similarly, we can obtain the 2Q and 3Q contributions by applying suitable intensity-cycling coefficients

$$\mathrm{PP}^{(2Q)} = \frac{1}{6}[\mathrm{PP}(4I_0) - \mathrm{PP}(3I_0) - \mathrm{PP}(I_0)] \tag{14}$$

$$\mathrm{PP}^{(3Q)} = \frac{1}{12}[\mathrm{PP}(4I_0) - 2\mathrm{PP}(3I_0) + 2\mathrm{PP}(I_0)] \tag{15}$$

In the case of very weak excitation, i.e., if $\mathrm{PP}(I)$ scaled linearly with the excitation intensity in the region from I_0 to $4I_0$, no higher-order signal would be present. In that case, only $\mathrm{PP}^{(3)}$ would contribute to $\mathrm{PP}^{(1Q)}$; that is, the $\mathrm{PP}^{(1Q)}$ signal would be contamination-free, equaling $\mathrm{PP}^{(3)}$, and $\mathrm{PP}^{(2Q)} \approx \mathrm{PP}^{(3Q)} \approx 0$. In the case of contamination with the $\mathrm{PP}^{(1Q)}$ signal, we can remove the higher-order contributions using eq 10. For example, fifth- and seventh-order contaminations can be corrected using the 2Q and 3Q signals by calculating

$$\mathrm{PP}^{(3)}I_0 = \mathrm{PP}^{(1Q)}(I_0) - 4\mathrm{PP}^{(2Q)}(I_0) + 9\mathrm{PP}^{(3Q)}(I_0) \tag{16}$$

Analogously, the contamination of seventh order at the 2Q position may be removed to obtain $\mathrm{PP}^{(5)}$.

Our method of higher-order PP spectroscopy thus offers a simple solution of correcting for contaminations by higher-order signals. If one is only interested in the clean third-order signal, the steps of isolation and correction for contamination can also be directly combined, i.e., essentially using eq 11, which for the present case of third order and $N = 3$ intensity-cycling steps reads

$$\mathrm{PP}^{(3)}I_0 = 2\mathrm{PP}(I_0) - \frac{2}{3}\mathrm{PP}(3I_0) + \frac{1}{4}\mathrm{PP}(4I_0) \tag{17}$$

This method provides a remarkably simple solution to the annihilation problem of ultrafast spectroscopy: Using eq 11 (or eq 16 or 17 for a useful special case), one instead employs a combination of excitation intensities to avoid the compromise, quantify the influence of higher orders, correct for them, and obtain clean third-order signals at high SNR. At the same time, one obtains "for free" the fifth- and seventh-order signals that provide additional information such as the dynamics of EEA in the system.

Contamination by higher-order signals occurs not only in PP but also in 2D spectroscopy. For example, the 1Q0Q1Q signal acquired in coherently detected 2D spectroscopy in PP geometry corresponds, at low excitation intensities, predominantly to a third-order signal. For higher excitation intensities, the 2Q0Q1Q signal dominated by fifth-order contributions can be isolated at $2\omega_0$, but at the same time, the 1Q0Q1Q signal will be contaminated with fifth-order contributions. For even higher excitation intensities, the 2Q0Q1Q signal will be contaminated by seventh-order contributions and the 1Q0Q1Q signal with fifth- and seventh-order contributions, and a 3Q0Q1Q signal appears at $3\omega_0$. In a similar way as in PP spectroscopy, the nQ signals in 2D spectroscopy can each be integrated along their own portion of the excitation frequency axis and then can be used to correct the lower-quantum signals and to isolate clean nonlinear orders.[58]

Simulating Higher-Order Spectra. While higher-order spectra do not need to be challenging to probe experimentally, they can be more challenging to study theoretically, especially as the order of the desired response increases. Some features can be read directly from the higher-order spectra, such as multiexciton binding energies,[46] but detailed prediction and interpretation of spectra generally requires simulation. Simulating nonlinear spectra requires (1) a model for the system under study, either a Hamiltonian or an open-systems formulation that includes interaction with a bath permitting dephasing and dissipation; (2) the interaction of the system with the semiclassical optical pulses, generally taken in the electric dipole approximation; and (3) specification of the experimental observable, whether it be coherently detected, fluorescence, or any other signal. These ingredients, in principle, allow simulation of any nonlinear optical spectroscopy experiment. There are two main routes to simulating such spectra. In nonperturbative simulations, the system evolves in time due to both its native propagation and its interaction with the optical pulses, where phase matching is simulated either with a spatially distributed set of systems or by a phase-cycling procedure.[81,96−98] Such simulations, as their name indicates, inherently include higher-order effects of the optical pulses and thus are not designed to extract the separate perturbative orders of the response of a system. But such an extraction could be performed using the same techniques described here and in our earlier publication[85] by calculating either several intensity-dependent PP simulations or windowed integration of separated nQ signals.[58]

In contrast, in perturbative calculations, the orders of light−matter interaction are separated perturbatively at the beginning. Such calculations are generally organized using double-sided Feynman diagrams.[6,56] The experimental observables determine a phase-discrimination condition, which limits the number of diagrams that must be considered at each order of perturbation theory.[99] Such diagrams make it straightforward to separate out the various nQ signals and orders of response. The number of diagrams that contribute to a desired signal can be small when the pulses do not overlap in time and in the rotating-wave approximation (RWA), but the number of diagrams grows rapidly with the order of the spectroscopy. In the case of coherently detected 2D spectroscopy with pump pulses that overlap in time (near $\tau = 0$) but with the third pulse well separated in time, the third-order response with the phase-matching condition $-\mathbf{k}_1 + \mathbf{k}_2 + \mathbf{k}_3$ in the RWA has 6 diagrams, corresponding to the stimulated emission, ground-state bleach, and excited-state absorption pathways. Under these same conditions, the fifth-order contribution to the 2Q0Q1Q signal ($-2\mathbf{k}_1 + 2\mathbf{k}_2 + \mathbf{k}_3$) has 54 diagrams and the seventh-order contribution to the 3Q0Q1Q signal ($-3\mathbf{k}_1 + 3\mathbf{k}_2 + \mathbf{k}_3$) has 570 diagrams.[58] If the third pulse also overlaps with the pump pulses, these diagram counts increase to 16, 240, and 3584 for the leading-order 1Q0Q1Q, 2Q0Q1Q, and 3Q0Q1Q responses, respectively. With particularly simple systems, these higher-order responses can be calculated analytically,[100,101] but most systems of interest require numerical evaluation, as does most consideration of the effects of finite pulse durations.

Writing down such large numbers of diagrams by hand is prone to error even before considering the calculations that each diagram represents. We have developed an automated Feynman diagram generator (DG) that produces double-sided Feynman diagrams.[99] The user inputs the phase-discrimination

https://doi.org/10.1021/acs.jpclett.3c01694
J. Phys. Chem. Lett. 2023, 14, 7556−7573

condition including the desired order of interaction with the pulses and which pulses overlap in time. The DG outputs a list of all of the diagrams that contribute, and it was used to determine the diagram counts mentioned just above. The DG is part of the freely available Ultrafast Software Suite (UFSS), a collection of modules that allows constructing the Hamiltonian or Liouvillian description of a system under study, the diagrams corresponding to a measurement, and the calculation of the signals produced from those diagrams, including the effects of pulse shapes and pulse overlaps.[99,102]

Each diagram represents a calculation of the quantum propagation of the system under study. Many time-domain propagation methods have been applied to make such calculations.[103−114] We instead perform the propagation computationally efficiently using the Ultrafast Ultrafast (UF^2) frequency-domain algorithm, which is part of UFSS. By diagonalizing the Hamiltonian or Liouvillian of the system once, the propagation of the system in the absence of the optical fields is computationally nearly costless, enabling rapid computation. UF^2 currently treats closed systems as well as open systems in the Redfield and Lindblad approximations. For systems in which the number of relevant Hamiltonian eigenstates is less than approximately 10000 (closed systems) or 100 (open systems), UF^2 is faster than competing time-domain direct-propagation methods, with speedups of over 2 orders of magnitude possible for many commonly considered small systems.[102,115]

We anticipate that the perturbative method will be particularly helpful for understanding spectra where the orders of response are separated, as in our recent publication[85] and as described in this Perspective. The perturbative method allows those responses to be calculated independently simply by choosing the set of desired diagrams. Even when the diagram counts become large, as in higher-order spectra with pulse overlaps, the UFSS enables efficient and accurate enumeration of the diagrams and calculation of the resulting signals.

Significance of Higher-Order Extraction. While we discussed the general meaning of higher-order signals in the beginning, let us conclude our discussion with some remarks on the physical significance of higher-order signals beyond the fifth order. Higher-order signals beyond fifth order can be obtained by choosing the appropriate intensity regime. Do they still provide useful additional information? For example, we performed higher-order PP spectroscopy on a squaraine polymer with measurements at six different intensities to isolate signals up to 13th order in perturbation theory.[85] In such polymers, the higher-order signals contain information about multiexciton interaction. In our example, we were able to determine the annihilation times for each specific number of simultaneously excited excitons by fitting the transients of the increasing orders of nonlinear signals, and thus, we obtained annihilation times for the biexciton, triexciton, and quadexciton from which we could in turn determine the probability of annihilation when two excitons meet. We found for the squaraine polymers that the annihilation rate increases with the number of simultaneous excitations, which makes intuitive sense because there are more possibilities for interactions when there are more excitons present and thus such interactions occur faster. However, we can go further and obtain quantitative information from higher orders. In our example of squaraine polymers, we could deduce that the excitons only annihilate with a chance of less than 10% when they pass near to each other. The conclusion of this result is that in the one-dimensional polymer chain, each exciton can in principle interact with all the other excitons that are present in the polymer, even if other excitons are initially "in between".[85] Our procedure of extracting clean nonlinear signals is general and can be extended to signals higher than 13th order by increasing the number of measured intensities beyond $N = 6$.

In summary, we demonstrated how fluorescence-detected and coherently detected higher-order multidimensional spectroscopy can be used to investigate phenomena inaccessible to lower-order spectroscopy. We provided examples of exciton−exciton annihilation (EEA) and highly excited states in quantum dots. An exciting new prospect is the extraction of higher orders directly from PP signals without having to resort to 2D techniques. This extraction exploits the dependence of the PP signal on the excitation intensity in a process that we call "intensity cycling" because it is derived from phase cycling for the case of a coincident pump pulse pair. Higher-order PP spectroscopy allows one to obtain clean orders of nonlinearity in transient absorption setups by simply changing the excitation intensity without the need to scan an additional time delay. This method solves the "annihilation problem" that plagued ultrafast spectroscopy for decades and thus helps to avoid errors in the assignment of time constants and the interpretation of kinetics for cases in which the excitation power cannot be chosen to be low enough to guarantee a clean third-order signal. Intensity cycling can be realized easily in any laboratory using a pair of rotatable polarizers or one polarizer and a half-wave plate. This technique allows one to measure annihilation-free transient absorption spectra under high excitation intensities, i.e., with a high SNR. One also obtains the higher-order responses "for free" along with the same data set. These higher orders allow experimenters to quantify exciton diffusion and the interaction probability when two excitons meet, as we demonstrated in the case of squaraine polymers, as well as giving spectral information about both singly and multiply excited states. Intensity-dependent and higher-order measurements have a long tradition in ultrafast spectroscopy, with many successful examples and sophisticated analysis. The new direction treated in this Perspective, however, is that nonlinear order extraction can be performed without requiring a priori models because the method is general.

Future Prospects. While so far we discussed mostly excitonic systems, our methods are not limited to excitons in molecular systems and can be applied to study other quasiparticles such as polaritons[116] or phonons.[117] One can use higher-order PP spectroscopy to observe multiparticle processes and characterize their individual time scales, interaction energies, and the involved states. Examples include, but are not limited to, multiexciton generation in quantum dots[118] or Auger recombination.[119] It was theoretically proposed to study a quantum system by systematically increasing the nonlinear order of excitation, i.e., by measuring increasing orders of the perturbative expansion.[120] Our developed techniques of higher-order PP and 2D spectroscopy can be viewed as the experimental realization of this theoretical concept, allowing us to systematically excite higher and higher states of a quantum system.

Before we discuss additional prospects for higher-order spectroscopic experiments, we want to address the general connection between higher-order nonlinear signals and spectral dimensionality. Since we have successfully analyzed higher-order signals in one and two spectral dimensions, we

https://doi.org/10.1021/acs.jpclett.3c01694
J. Phys. Chem. Lett. 2023, 14, 7556−7573

may ask: Do we additionally need higher spectral dimensionality to fully interpret higher-order signals? In the standard implementation of third-order 2D spectroscopy, each laser pulse interacts once with the system (and analogously for fourth-order fluorescence-detected 2D spectroscopy with four pulses). With pulses shorter than the electronic (and vibrational) dynamics, nonlinear spectroscopy experiments take place in a mostly "impulsive" limit, i.e., the pulses act as effective delta functions in time, and the nonlinear response of the sample is directly probed in the time domain. The light−matter interactions are ordered in time, and the language of response pathways, depicted by double-sided Feynman diagrams, is typically used. In four-wave-mixing 2D spectroscopy, the experimenter thus has full control over all time delays of the response function. To extend this control into higher orders of nonlinearity, one additional pulse would have to be used for each additional interaction in the perturbative description (i.e., five pulses in fifth-order coherent spectroscopy, six pulses in sixth-order action-detected spectroscopy, etc.). This approach has been realized in collinear geometry using phase cycling[49,121] and in noncollinear geometry using phase matching for a fifth-order (six-wave mixing) signal.[122] The resulting spectra are highly multidimensional (four dimensional in the case of fifth-order response), which requires scanning of all interpulse delays, making the experiment conceptually and practically challenging. While the data contain a wealth of information, the multidimensionality typically makes it necessary to resort to spectral- and time-domain cuts or spectral projections to facilitate interpretation. Because of the Fourier-transform relationship between the time and frequency domains, spectral projections can be realized directly by measuring at zero time delay with multiple interactions with a single pulse (projection-slice theorem). The best-known example is a PP spectrum that emerges as a projection of a third-order 2D spectrum as we discussed in the context of higher-order PP spectroscopy.[85] One then benefits from a significant dimensionality reduction when carrying out higher-order PP spectroscopy using just one pair of pulses rather than having to scan many individual delay times. This choice leads to a simplification of the experiment, reduction of measurement time, and, to an extent, a simplification of the interpretation as well.[123]

Measuring at reduced dimensionality has the disadvantage that the spectral information becomes more congested. As demonstrated recently, polarization control can still be used to isolate specific contributions,[68] or intensity cycling as explained in the present work allows isolating orders of nonlinearity despite "too low" dimensionality.[85] Despite the great advantages due to the simplicity, some information content is not resolved, e.g., the excitation line shape in the case of PP. In the context of these opposing motivations, we see two directions for future higher-order experiments. First, the acquisition of higher-order multidimensional spectra could be combined with fully automated measurement and possibly automated data processing that precedes interpretation. This preanalysis would help to find the relevant projections and correlations. Data processing and interpretation can be combined with machine learning. Early examples demonstrated the power of neural networks to predict the system response for phase-shaped femtosecond pulses,[124,125] while recent examples utilized machine learning to study multidimensional spectra.[126] Recent technical improvements such as high-repetition-rate setups and fast data acquisition should make it possible to measure signals of high dimensionality in a reasonable amount of time. One particular example is shot-to-shot pulse shaping using laser systems with 100 kHz repetition rates[74] that can be combined with many-step phase cycling to obtain large-scale data sets in a reasonable amount of time. As a second approach to dealing with the large amount of data in higher-order experiments, one can resort to measuring projections on relevant subspaces of the multidimensional spectral response. While we have investigated projections that correspond to overlapping pulse pairs, one might envision other scenarios employing more complex pulse shapes for exploring the nonlinear response function, a topic that was explored in the field of quantum control.[127,128] Such scenarios still hold significant potential in combination with multidimensional spectroscopy, in particular, in the context of separating nonlinear orders systematically even with excitation-frequency resolution.

An obvious extension of higher-order spectroscopy beyond bulk measurements is its combination with spatial resolution. Multidimensional spectroscopy has already been combined with fluorescence microscopy.[75,129] Another variant combines action-detected phase-cycling 2D spectroscopy with photoemission electron microscopy (PEEM), providing spatial resolution down to ∼3 nm, which is why we named it "2D nanoscopy".[15,16] 2D nanoscopy allowed us to detect a plasmon-polariton quantum wave packet.[130] In this example, we observed aliased 3Q coherences in an eighth-order nonlinear process that could be assigned to multiple excitations of the plasmon. This example demonstrates that higher-order signals also play an important role in plasmonic systems. In the future, 2D fluorescence microscopy or 2D nanoscopy could be combined with higher phase-cycling schemes to isolate higher-order signals. Such experiments would allow us to obtain spatially varying local properties, such as the annihilation times and properties and dynamics of highly excited states. Apart from 2D spectroscopy, higher-order PP spectroscopy using intensity cycling could be easily implemented with a microscope. Such an approach could be used to characterize the spatial variations of (multi)exciton dynamics within a sample. Understanding the local excitonic properties is important for the development of optoelectronic devices based on organic molecules. For any device, the processing into thin films or bulk materials can result in different phases that contain varying local structures and thus modified interactions between the constituents (i.e., molecules). Such processing typically leads to a change of properties from solution to bulk material contained in an actual device.[131,132] Spatially resolved higher-order spectroscopy could characterize the local properties and determine the influence of local structure, such as in domains, at interfaces, or around local defects. For example, one might envision using fifth-order spectroscopy to resolve the local spatial variations in exciton diffusion within a thin film.

Another future development could be two-color experiments such as in (third-order) 2D electronic−vibrational (2DEV)[133,134] or 2D vibrational−electronic (2DVE) spectroscopy.[135] In current 2DEV experiments, the system is excited with a double pulse in the visible regime followed by a mid-infrared probe pulse, allowing one to follow the evolution of the excited states by their vibrational signature. Increasing the excitation intensity of the pump pulses would generate a 2Q coherence or higher coherence with the first pulse and hence grant access to highly excited states. Probing with an infrared

https://doi.org/10.1021/acs.jpclett.3c01694
J. Phys. Chem. Lett. 2023, 14, 7556−7573

pulse could then be used to study the vibrations of highly excited states and to investigate the localization of the state by its specific vibrational signature.

We live in a strongly entangled universe: we often separate our object of investigation into a "system" and an "environment" whose interaction leads to aspects of entanglement, decoherence, and the emergence of a classical world from quantum mechanics.[136] In order to deal with the complexity of the real world, we often resort to the use of single-particle pictures. For example, we treat multielectron atoms by assuming a single-particle picture that leads to the establishment of (useful) atomic orbitals, or we assume a single-particle picture to arrive at the band structure of semiconductors. This concept is certainly very powerful but ignores an important part of physics. Correlation phenomena abound in many areas of science, from describing molecular properties to superconductivity.[137−139] These correlations reflect the fact that the fundamental quantum wave function of a multiparticle system depends on the coordinates of all constituents and can, in general, not be written as a product of single-particle wave functions, except for special cases and approximations. Thus, in order to understand multiparticle wave functions, we need tools to investigate the interactions between their constituents. We argue that higher-order multidimensional and pump−probe spectroscopies, as outlined in this Perspective, provide such tools because they offer a comprehensive approach to decipher particle and quasiparticle correlations in systematically increasing orders of interaction and on ultrafast time scales.

AUTHOR INFORMATION

Corresponding Author

Tobias Brixner − *Institut für Physikalische und Theoretische Chemie, Universität Würzburg, 97074 Würzburg, Germany; Center for Nanosystems Chemistry (CNC), Universität Würzburg, 97074 Würzburg, Germany;* orcid.org/0000-0002-6529-704X; Email: brixner@uni-wuerzburg.de

Authors

Julian Lüttig − *Institut für Physikalische und Theoretische Chemie, Universität Würzburg, 97074 Würzburg, Germany;* orcid.org/0009-0009-4926-2689

Stefan Mueller − *Institut für Physikalische und Theoretische Chemie, Universität Würzburg, 97074 Würzburg, Germany*

Pavel Malý − *Institut für Physikalische und Theoretische Chemie, Universität Würzburg, 97074 Würzburg, Germany; Faculty of Mathematics and Physics, Charles University, 121 16 Prague, Czech Republic;* orcid.org/0000-0001-9244-9718

Jacob J. Krich − *Department of Physics and School of Electrical Engineering and Computer Science, University of Ottawa, Ottawa K1N 6N5, Canada;* orcid.org/0000-0003-4514-0720

Complete contact information is available at: https://pubs.acs.org/10.1021/acs.jpclett.3c01694

Notes

The authors declare no competing financial interest.

Biographies

Julian Lüttig obtained his Ph.D. in Chemistry from the University of Würzburg in 2022. During his Ph.D., he focused on the development and application of coherently detected higher-order spectroscopy. He is currently a postdoctoral research fellow in the group of Prof. Ogilvie at the University of Michigan.

Stefan Mueller is a research associate in the group of Tobias Brixner. His Ph.D. thesis (completed in 2021 at the University of Würzburg) was on "Coherent Multiple-Quantum Multidimensional Fluorescence Spectroscopy".

Pavel Malý got his Ph.D. at Vrije Universiteit Amsterdam and Charles University in Prague in 2018. After a postdoc at University of Würzburg, he returned to Prague. He uses ultrafast and single-molecule spectroscopy to study complex molecular systems.

Jacob J. Krich is an Associate Professor at the University of Ottawa in the Department of Physics with a cross-appointment to the School of Electrical Engineering and Computer Science. He received his Ph.D. in theoretical condensed matter physics from Harvard University, and his research focuses on nonlinear spectroscopies of organic systems and novel pathways to high-efficiency photovoltaics.

In his Ph.D. thesis, **Tobias Brixner** developed adaptive quantum control and pulse shaping concepts, and as a postdoc with Graham Fleming at Berkeley, he recorded the first 2D electronic spectrum of a multichromophore system. He has been a Full Professor of Physical Chemistry and Physics at the University of Würzburg since 2007 and focuses on the development of ultrafast spectroscopy methods with applications to liquid, solid, and molecular beam samples.

ACKNOWLEDGMENTS

We acknowledge funding from the Deutsche Forschungsgemeinschaft (DFG, German Research Foundation) (Grant No. 423942615 − T.B.). J.J.K. acknowledges support from the Canadian Natural Sciences and Engineering Research Council. J.L. was supported by a scholarship of the Cusanuswerk. P.M. acknowledges support by the Alexander von Humboldt Foundation.

REFERENCES

(1) Tiwari, V. Multidimensional Electronic Spectroscopy in High-Definition—Combining Spectral, Temporal, and Spatial Resolutions. *J. Chem. Phys.* **2021**, *154* (23), 230901.

(2) Biswas, S.; Kim, J.; Zhang, X.; Scholes, G. D. Coherent Two-Dimensional and Broadband Electronic Spectroscopies. *Chem. Rev.* **2022**, *122* (3), 4257−4321.

(3) Shim, S.-H.; Zanni, M. T. How to Turn Your Pump−Probe Instrument into a Multidimensional Spectrometer: 2D IR and VIS Spectroscopies via Pulse Shaping. *Phys. Chem. Chem. Phys.* **2009**, *11* (5), 748−761.

(4) Augulis, R.; Zigmantas, D. Two-Dimensional Electronic Spectroscopy with Double Modulation Lock-in Detection: Enhancement of Sensitivity and Noise Resistance. *Opt. Express* **2011**, *19* (14), 13126−13133.

(5) Fuller, F. D.; Wilcox, D. E.; Ogilvie, J. P. Pulse Shaping Based Two-Dimensional Electronic Spectroscopy in a Background Free Geometry. *Opt. Express* **2014**, *22* (1), 1018.

(6) Hamm, P.; Zanni, M. *Concepts and Methods of 2D Infrared Spectroscopy*, 1st ed.; Cambridge University Press: New York, 2011. DOI: 10.1017/CBO9780511675935.

(7) Cho, M. Coherent Nonlinear Spectroscopy with Multiple Mode-Locked Lasers. *J. Phys. Chem. Lett.* **2021**, *12* (42), 10284−10294.

(8) Skoff, D. R.; Laaser, J. E.; Mukherjee, S. S.; Middleton, C. T.; Zanni, M. T. Simplified and Economical 2D IR Spectrometer Design Using a Dual Acousto-Optic Modulator. *Chem. Phys.* **2013**, *422*, 8−15.

(9) Malý, P.; Lüttig, J.; Mueller, S.; Schreck, M. H.; Lambert, C.; Brixner, T. Coherently and Fluorescence-Detected Two-Dimensional Electronic Spectroscopy: Direct Comparison on Squaraine Dimers. *Phys. Chem. Chem. Phys.* **2020**, *22* (37), 21222−21237.

(10) Tian, P.; Keusters, D.; Suzaki, Y.; Warren, W. S. Femtosecond Phase-Coherent Two-Dimensional Spectroscopy. *Science* **2003**, *300* (5625), 1553−1555.
(11) Tekavec, P. F.; Lott, G. A.; Marcus, A. H. Fluorescence-Detected Two-Dimensional Electronic Coherence Spectroscopy by Acousto-Optic Phase Modulation. *J. Chem. Phys.* **2007**, *127* (21), 214307.
(12) De, A. K.; Monahan, D.; Dawlaty, J. M.; Fleming, G. R. Two-Dimensional Fluorescence-Detected Coherent Spectroscopy with Absolute Phasing by Confocal Imaging of a Dynamic Grating and 27-Step Phase-Cycling. *J. Chem. Phys.* **2014**, *140* (19), 194201.
(13) Tiwari, V.; Matutes, Y. A.; Konar, A.; Yu, Z.; Ptaszek, M.; Bocian, D. F.; Holten, D.; Kirmaier, C.; Ogilvie, J. P. Strongly Coupled Bacteriochlorin Dyad Studied Using Phase-Modulated Fluorescence-Detected Two-Dimensional Electronic Spectroscopy. *Opt. Express* **2018**, *26* (17), 22327−22341.
(14) Karki, K. J.; Chen, J.; Sakurai, A.; Shi, Q.; Gardiner, A. T.; Kühn, O.; Cogdell, R. J.; Pullerits, T. Before Förster. Initial Excitation in Photosynthetic Light Harvesting. *Chem. Sci.* **2019**, *10*, 7923−7928.
(15) Aeschlimann, M.; Brixner, T.; Fischer, A.; Kramer, C.; Melchior, P.; Pfeiffer, W.; Schneider, C.; Strüber, C.; Tuchscherer, P.; Voronine, D. V. Coherent Two-Dimensional Nanoscopy. *Science* **2011**, *333* (6050), 1723−1726.
(16) Huber, B.; Pres, S.; Wittmann, E.; Dietrich, L.; Lüttig, J.; Fersch, D.; Krauss, E.; Friedrich, D.; Kern, J.; Lisinetskii, V.; Hensen, M.; Hecht, B.; Bratschitsch, R.; Riedle, E.; Brixner, T. Space- and Time-Resolved UV-to-NIR Surface Spectroscopy and 2D Nanoscopy at 1 MHz Repetition Rate. *Rev. Sci. Instrum.* **2019**, *90* (11), 113103.
(17) Uhl, D.; Bangert, U.; Bruder, L.; Stienkemeier, F. Coherent Optical 2D Photoelectron Spectroscopy. *Optica* **2021**, *8* (10), 1316−1324.
(18) Roeding, S.; Brixner, T. Coherent Two-Dimensional Electronic Mass Spectrometry. *Nat. Commun.* **2018**, *9* (1), 2519.
(19) Bruder, L.; Bangert, U.; Binz, M.; Uhl, D.; Vexiau, R.; Bouloufa-Maafa, N.; Dulieu, O.; Stienkemeier, F. Coherent Multidimensional Spectroscopy of Dilute Gas-Phase Nanosystems. *Nat. Commun.* **2018**, *9* (1), 4823.
(20) Solowan, H.-P.; Malý, P.; Brixner, T. Direct Comparison of Molecular-Beam vs Liquid-Phase Pump−Probe and Two-Dimensional Spectroscopy on the Example of Azulene. *J. Chem. Phys.* **2022**, *157* (4), No. 044201.
(21) Nardin, G.; Autry, T. M.; Silverman, K. L.; Cundiff, S. T. Multidimensional Coherent Photocurrent Spectroscopy of a Semiconductor Nanostructure. *Opt. Express* **2013**, *21* (23), 28617−28627.
(22) Karki, K. J.; Widom, J. R.; Seibt, J.; Moody, I.; Lonergan, M. C.; Pullerits, T.; Marcus, A. H. Coherent Two-Dimensional Photocurrent Spectroscopy in a PbS Quantum Dot Photocell. *Nat. Commun.* **2014**, *5*, 5869.
(23) Bakulin, A. A.; Silva, C.; Vella, E. Ultrafast Spectroscopy with Photocurrent Detection: Watching Excitonic Optoelectronic Systems at Work. *J. Phys. Chem. Lett.* **2016**, *7* (2), 250−258.
(24) Bolzonello, L.; Bernal-Texca, F.; Gerling, L. G.; Ockova, J.; Collini, E.; Martorell, J.; van Hulst, N. F. Photocurrent-Detected 2D Electronic Spectroscopy Reveals Ultrafast Hole Transfer in Operating PM6/Y6 Organic Solar Cells. *J. Phys. Chem. Lett.* **2021**, *12* (16), 3983−3988.
(25) Thyrhaug, E.; Žídek, K.; Dostál, J.; Bína, D.; Zigmantas, D. Exciton Structure and Energy Transfer in the Fenna−Matthews−Olson Complex. *J. Phys. Chem. Lett.* **2016**, *7* (9), 1653−1660.
(26) Bixner, O.; Lukeš, V.; Mančal, T.; Hauer, J.; Milota, F.; Fischer, M.; Pugliesi, I.; Bradler, M.; Schmid, W.; Riedle, E.; Kauffmann, H. F.; Christensson, N. Ultrafast Photo-Induced Charge Transfer Unveiled by Two-Dimensional Electronic Spectroscopy. *J. Chem. Phys.* **2012**, *136* (20), 204503.
(27) Malý, P.; Mančal, T. Signatures of Exciton Delocalization and Exciton−Exciton Annihilation in Fluorescence-Detected Two-Dimensional Coherent Spectroscopy. *J. Phys. Chem. Lett.* **2018**, *9*, 5654−5659.
(28) Kühn, O.; Mančal, T.; Pullerits, T. Interpreting Fluorescence Detected Two-Dimensional Electronic Spectroscopy. *J. Phys. Chem. Lett.* **2020**, *11* (3), 838−842.
(29) Dostál, J.; Pšenčík, J.; Zigmantas, D. In Situ Mapping of the Energy Flow through the Entire Photosynthetic Apparatus. *Nat. Chem.* **2016**, *8*, 705−710.
(30) Mančal, T.; Christensson, N.; Lukeš, V.; Milota, F.; Bixner, O.; Kauffmann, H. F.; Hauer, J. System-Dependent Signatures of Electronic and Vibrational Coherences in Electronic Two-Dimensional Spectra. *J. Phys. Chem. Lett.* **2012**, *3* (11), 1497−1502.
(31) Butkus, V.; Alster, J.; Bašinskaitė, E.; Augulis, R.; Neuhaus, P.; Valkunas, L.; Anderson, H. L.; Abramavicius, D.; Zigmantas, D. Discrimination of Diverse Coherences Allows Identification of Electronic Transitions of a Molecular Nanoring. *J. Phys. Chem. Lett.* **2017**, *8* (10), 2344−2349.
(32) Do, T. N.; Khyasudeen, M. F.; Nowakowski, P. J.; Zhang, Z.; Tan, H. Measuring Ultrafast Spectral Diffusion and Correlation Dynamics by Two-dimensional Electronic Spectroscopy. *Chem. Asian J.* **2019**, *14* (22), 3992−4000.
(33) Kriete, B.; Bondarenko, A. S.; Alessandri, R.; Patmanidis, I.; Krasnikov, V. V.; Jansen, T. L. C.; Marrink, S. J.; Knoester, J.; Pshenichnikov, M. S. Molecular versus Excitonic Disorder in Individual Artificial Light-Harvesting Systems. *J. Am. Chem. Soc.* **2020**, *142* (42), 18073−18085.
(34) Milota, F.; Prokhorenko, V. I.; Mancal, T.; von Berlepsch, H.; Bixner, O.; Kauffmann, H. F.; Hauer, J. Vibronic and Vibrational Coherences in Two-Dimensional Electronic Spectra of Supramolecular J-Aggregates. *J. Phys. Chem. A* **2013**, *117* (29), 6007−6014.
(35) Nuernberger, P.; Ruetzel, S.; Brixner, T. Multidimensional Electronic Spectroscopy of Photochemical Reactions. *Angew. Chem., Int. Ed.* **2015**, *54* (39), 11368−11386.
(36) Policht, V. R.; Russo, M.; Liu, F.; Trovatello, C.; Maiuri, M.; Bai, Y.; Zhu, X.; Dal Conte, S.; Cerullo, G. Dissecting Interlayer Hole and Electron Transfer in Transition Metal Dichalcogenide Heterostructures via Two-Dimensional Electronic Spectroscopy. *Nano Lett.* **2021**, *21* (11), 4738−4743.
(37) Cundiff, S. T.; Zhang, T.; Bristow, A. D.; Karaiskaj, D.; Dai, X. Optical Two-Dimensional Fourier Transform Spectroscopy of Semiconductor Quantum Wells. *Acc. Chem. Res.* **2009**, *42* (9), 1423−1432.
(38) Trinkunas, G.; Herek, J. L.; Polívka, T.; Sundström, V.; Pullerits, T. Exciton Delocalization Probed by Excitation Annihilation in the Light-Harvesting Antenna LH2. *Phys. Rev. Lett.* **2001**, *86* (18), 4167−4170.
(39) Völker, S. F.; Schmiedel, A.; Holzapfel, M.; Renziehausen, K.; Engel, V.; Lambert, C. Singlet−Singlet Exciton Annihilation in an Exciton-Coupled Squaraine-Squaraine Copolymer: A Model toward Hetero-J-Aggregates. *J. Phys. Chem. C* **2014**, *118* (31), 17467−17482.
(40) Pšenčík, J.; Ma, Y.-Z.; Arellano, J. B.; Hála, J.; Gillbro, T. Excitation Energy Transfer Dynamics and Excited-State Structure in Chlorosomes of Chlorobium Phaeobacteroides. *Biophys. J.* **2003**, *84* (2), 1161−1179.
(41) Müller, M. G.; Lambrev, P.; Reus, M.; Wientjes, E.; Croce, R.; Holzwarth, A. R. Singlet Energy Dissipation in the Photosystem II Light-Harvesting Complex Does Not Involve Energy Transfer to Carotenoids. *ChemPhysChem* **2010**, *11* (6), 1289−1296.
(42) Gulbinas, V.; Valkunas, L.; Kuciauskas, D.; Katilius, E.; Liuolia, V.; Zhou, W.; Blankenship, R. E. Singlet−Singlet Annihilation and Local Heating in FMO Complexes. *J. Phys. Chem.* **1996**, *100* (45), 17950−17956.
(43) Sundström, V.; Gillbro, T.; Gadonas, R. A.; Piskarskas, A. Annihilation of Singlet Excitons in J Aggregates of Pseudoisocyanine (PIC) Studied by Pico- and Subpicosecond Spectroscopy. *J. Chem. Phys.* **1988**, *89* (5), 2754−2762.
(44) Fennel, F.; Lochbrunner, S. Exciton-Exciton Annihilation in a Disordered Molecular System by Direct and Multistep Förster Transfer. *Phys. Rev. B* **2015**, *92* (14), No. 140301.
(45) Valkunas, L.; Akesson, E.; Pullerits, T.; Sundström, V. Energy Migration in the Light-Harvesting Antenna of the Photosynthetic

https://doi.org/10.1021/acs.jpclett.3c01694
J. Phys. Chem. Lett. 2023, 14, 7556−7573

Bacterium Rhodospirillum Rubrum Studied by Time-Resolved Excitation Annihilation at 77 K. *Biophys. J.* **1996**, *70* (5), 2373−2379.
(46) Turner, D. B.; Nelson, K. A. Coherent Measurements of High-Order Electronic Correlations in Quantum Wells. *Nature* **2010**, *466* (7310), 1089−1092.
(47) Zhang, Z.; Lambrev, P. H.; Wells, K. L.; Garab, G.; Tan, H.-S. Direct Observation of Multistep Energy Transfer in LHCII with Fifth-Order 3D Electronic Spectroscopy. *Nat. Commun.* **2015**, *6*, 7914.
(48) Ding, F.; Fulmer, E. C.; Zanni, M. T. Heterodyned Fifth-Order Two-Dimensional IR Spectroscopy: Third-Quantum States and Polarization Selectivity. *J. Chem. Phys.* **2005**, *123* (9), No. 094502.
(49) Zhang, Z.; Wells, K. L.; Seidel, M. T.; Tan, H.-S. Fifth-Order Three-Dimensional Electronic Spectroscopy Using a Pump−Probe Configuration. *J. Phys. Chem. B* **2013**, *117* (49), 15369−15385.
(50) Fulmer, E. C.; Ding, F.; Zanni, M. T. Heterodyned Fifth-Order 2D-IR Spectroscopy of the Azide Ion in an Ionic Glass. *J. Chem. Phys.* **2005**, *122* (3), No. 034302.
(51) Fidler, A. F.; Harel, E.; Engel, G. S. Dissecting Hidden Couplings Using Fifth-Order Three-Dimensional Electronic Spectroscopy. *J. Phys. Chem. Lett.* **2010**, *1* (19), 2876−2880.
(52) Brosseau, P.; Palato, S.; Seiler, H.; Baker, H.; Kambhampati, P. Fifth-Order Two-Quantum Absorptive Two-Dimensional Electronic Spectroscopy of CdSe Quantum Dots. *J. Chem. Phys.* **2020**, *153* (23), 234703.
(53) Wu, H.; Berg, M. A. Multiple Population-Period Transient Spectroscopy (MUPPETS) in Excitonic Systems. *J. Chem. Phys.* **2013**, *138* (3), No. 034201.
(54) Malý, P.; Mueller, S.; Lüttig, J.; Lambert, C.; Brixner, T. Signatures of Exciton Dynamics and Interaction in Coherently and Fluorescence-Detected Four- and Six-Wave-Mixing Two-Dimensional Electronic Spectroscopy. *J. Chem. Phys.* **2020**, *153* (14), 144204.
(55) Mueller, S.; Brixner, T. Molecular Coherent Three-Quantum Two-Dimensional Fluorescence Spectroscopy. *J. Phys. Chem. Lett.* **2020**, *11* (13), 5139−5147.
(56) Mukamel, S. *Principles of Nonlinear Optical Spectroscopy*, 1st ed.; Oxford University Press: New York, 1995.
(57) Bukartė, E.; Paleček, D.; Edlund, P.; Westenhoff, S.; Zigmantas, D. Dynamic Band-Shift Signal in Two-Dimensional Electronic Spectroscopy: A Case of Bacterial Reaction Center. *J. Chem. Phys.* **2021**, *154* (11), 115102.
(58) Lüttig, J.; Malý, P.; Rose, P. A.; Turkin, A.; Bühler, M.; Lambert, C.; Krich, J. J.; Brixner, T. High-Order Pump−Probe and High-Order Two-Dimensional Electronic Spectroscopy on the Example of Squaraine Oligomers. *J. Chem. Phys.* **2023**, *158* (23), 234201.
(59) Mueller, S.; Lüttig, J.; Malý, P.; Ji, L.; Han, J.; Moos, M.; Marder, T. B.; Bunz, U. H. F.; Dreuw, A.; Lambert, C.; Brixner, T. Rapid Multiple-Quantum Three-Dimensional Fluorescence Spectroscopy Disentangles Quantum Pathways. *Nat. Commun.* **2019**, *10*, 4735.
(60) Heshmatpour, C.; Malevich, P.; Plasser, F.; Menger, M.; Lambert, C.; Šanda, F.; Hauer, J. Annihilation Dynamics of Molecular Excitons Measured at a Single Perturbative Excitation Energy. *J. Phys. Chem. Lett.* **2020**, *11* (18), 7776−7781.
(61) Agathangelou, D.; Javed, A.; Sessa, F.; Solinas, X.; Joffre, M.; Ogilvie, J. P. Phase-Modulated Rapid-Scanning Fluorescence-Detected Two-Dimensional Electronic Spectroscopy. *J. Chem. Phys.* **2021**, *155* (9), No. 094201.
(62) Yu, S.; Geng, Y.; Liang, D.; Li, H.; Liu, X. Double-Quantum−Zero-Quantum 2D Coherent Spectroscopy Reveals Quantum Coherence between Collective States in an Atomic Vapor. *Opt. Lett.* **2022**, *47* (4), 997−1000.
(63) Autry, T. M.; Moody, G.; Fraser, J.; McDonald, C.; Mirin, R. P.; Silverman, K. Single-Scan Acquisition of Multiple Multidimensional Spectra. *Optica* **2019**, *6* (6), 735.
(64) Dostál, J.; Fennel, F.; Koch, F.; Herbst, S.; Würthner, F.; Brixner, T. Direct Observation of Exciton−Exciton Interactions. *Nat. Commun.* **2018**, *9* (1), 2466.
(65) DeFlores, L. P.; Nicodemus, R. A.; Tokmakoff, A. Two-Dimensional Fourier Transform Spectroscopy in the Pump-Probe Geometry. *Opt. Lett.* **2007**, *32* (20), 2966−2968.
(66) Ninck, M.; Galler, A.; Feurer, T.; Brixner, T. Programmable Common-Path Vector Field Synthesizer for Femtosecond Pulses. *Opt. Lett.* **2007**, *32* (23), 3379−3381.
(67) Schwarz, C.; Hüter, O.; Brixner, T. Full Vector-Field Control of Ultrashort Laser Pulses Utilizing a Single Dual-Layer Spatial Light Modulator in a Common-Path Setup. *J. Opt. Soc. Am. B* **2015**, *32* (5), 933−945.
(68) Farrell, K. M.; Yang, N.; Zanni, M. T. A Polarization Scheme That Resolves Cross-Peaks with Transient Absorption and Eliminates Diagonal Peaks in 2D Spectroscopy. *Proc. Natl. Acad. Sci. U. S. A.* **2022**, *119* (6), No. e2117398119.
(69) Yan, S.; Tan, H.-S. Phase Cycling Schemes for Two-Dimensional Optical Spectroscopy with a Pump−Probe Beam Geometry. *Chem. Phys.* **2009**, *360* (1−3), 110−115.
(70) Draeger, S.; Roeding, S.; Brixner, T. Rapid-Scan Coherent 2D Fluorescence Spectroscopy. *Opt. Express* **2017**, *25* (4), 3259−3267.
(71) Fersch, D.; Malý, P.; Rühe, J.; Lisinetskii, V.; Hensen, M.; Würthner, F.; Brixner, T. Single-Molecule Ultrafast Fluorescence-Detected Pump−Probe Microscopy. *J. Phys. Chem. Lett.* **2023**, *14*, 4923−4932.
(72) Bain, A. D. Coherence Levels and Coherence Pathways in NMR. A Simple Way to Design Phase Cycling Procedures. *Journal of Magnetic Resonance (1969)* **1984**, *56* (3), 418−427.
(73) Tan, H.-S. Theory and Phase-Cycling Scheme Selection Principles of Collinear Phase Coherent Multi-Dimensional Optical Spectroscopy. *J. Chem. Phys.* **2008**, *129* (12), 124501.
(74) Kearns, N. M.; Mehlenbacher, R. D.; Jones, A. C.; Zanni, M. T. Broadband 2D Electronic Spectrometer Using White Light and Pulse Shaping: Noise and Signal Evaluation at 1 and 100 kHz. *Opt. Express* **2017**, *25* (7), 7869−7883.
(75) Goetz, S.; Li, D.; Kolb, V.; Pflaum, J.; Brixner, T. Coherent Two-Dimensional Fluorescence Micro-Spectroscopy. *Opt. Express* **2018**, *26* (4), 3915−3925.
(76) Pres, S.; Kontschak, L.; Hensen, M.; Brixner, T. Coherent 2D Electronic Spectroscopy with Complete Characterization of Excitation Pulses during All Scanning Steps. *Opt. Express* **2021**, *29* (3), 4191−4209.
(77) Mueller, S.; Draeger, S.; Ma, X.; Hensen, M.; Kenneweg, T.; Pfeiffer, W.; Brixner, T. Fluorescence-Detected Two-Quantum and One-Quantum−Two-Quantum 2D Electronic Spectroscopy. *J. Phys. Chem. Lett.* **2018**, *9* (8), 1964−1969.
(78) Mueller, S.; Lüttig, J.; Brenneis, L.; Oron, D.; Brixner, T. Observing Multiexciton Correlations in Colloidal Semiconductor Quantum Dots via Multiple-Quantum Two-Dimensional Fluorescence Spectroscopy. *ACS Nano* **2021**, *15* (3), 4647−4657.
(79) Jayachandran, A.; Mueller, S.; Brixner, T. Fluorescence-Detected Two-Quantum Photon Echoes via Cogwheel Phase Cycling. *J. Phys. Chem. Lett.* **2022**, *13* (50), 11710−11719.
(80) Kumar, S.; Dunn, I. S.; Deng, S.; Zhu, T.; Zhao, Q.; Williams, O. F.; Tempelaar, R.; Huang, L. Exciton Annihilation in Molecular Aggregates Suppressed through Quantum Interference. *Nat. Chem.* **2023**, *15*, 1118.
(81) Brüggemann, B.; May, V. Exciton Exciton Annihilation Dynamics in Chromophore Complexes. II. Intensity Dependent Transient Absorption of the LH2 Antenna System. *J. Chem. Phys.* **2004**, *120* (5), 2325−2336.
(82) Malý, P.; Lüttig, J.; Turkin, A.; Dostál, J.; Lambert, C.; Brixner, T. From Wavelike to Sub-Diffusive Motion: Exciton Dynamics and Interaction in Squaraine Copolymers of Varying Length. *Chem. Sci.* **2020**, *11* (2), 456−466.
(83) Lüttig, J.; Brixner, T.; Malý, P. Anisotropy in Fifth-Order Exciton−Exciton-Interaction Two-Dimensional Spectroscopy. *J. Chem. Phys.* **2021**, *154* (15), 154202.
(84) Heshmatpour, C.; Hauer, J.; Šanda, F. Interplay of Exciton Annihilation and Transport in Fifth Order Electronic Spectroscopy. *Chem. Phys.* **2020**, *528*, No. 110433.

https://doi.org/10.1021/acs.jpclett.3c01694
J. Phys. Chem. Lett. 2023, 14, 7556−7573

(85) Malý, P.; Lüttig, J.; Rose, P. A.; Turkin, A.; Lambert, C.; Krich, J. J.; Brixner, T. Separating Single- from Multi-Particle Dynamics in Nonlinear Spectroscopy. *Nature* **2023**, *616*, 280−287.
(86) Mikhnenko, O. V.; Blom, P. W. M.; Nguyen, T.-Q. Exciton Diffusion in Organic Semiconductors. *Energy Environ. Sci.* **2015**, *8* (7), 1867−1888.
(87) Jin, X.-H.; Price, M. B.; Finnegan, J. R.; Boott, C. E.; Richter, J. M.; Rao, A.; Menke, S. M.; Friend, R. H.; Whittell, G. R.; Manners, I. Long-Range Exciton Transport in Conjugated Polymer Nanofibers Prepared by Seeded Growth. *Science* **2018**, *360* (6391), 897−900.
(88) Kriete, B.; Lüttig, J.; Kunsel, T.; Malý, P.; Jansen, T. L. C.; Knoester, J.; Brixner, T.; Pshenichnikov, M. S. Interplay between Structural Hierarchy and Exciton Diffusion in Artificial Light Harvesting. *Nat. Commun.* **2019**, *10* (1), 4615.
(89) Heshmatpour, C.; Hauer, J.; Sanda, F. Correlated Spectral Fluctuations Quantified by Lineshape Analysis of Fifth Order Two-Dimensional Electronic Spectra. *J. Chem. Phys.* **2022**, *156* (8), No. 084114.
(90) Malý, P.; Mueller, S.; Lüttig, J.; Lambert, C.; Brixner, T. Signatures of Exciton Dynamics and Interaction in Coherently and Fluorescence-Detected Four- and Six-Wave-Mixing Two-Dimensional Electronic Spectroscopy. *J. Chem. Phys.* **2020**, *153* (14), 144204.
(91) Mueller, S.; Brixner, T. Molecular Coherent Three-Quantum Two-Dimensional Fluorescence Spectroscopy. *J. Phys. Chem. Lett.* **2020**, *11* (13), 5139−5147.
(92) Gallagher Faeder, S. M.; Jonas, D. M. Two-Dimensional Electronic Correlation and Relaxation Spectra: Theory and Model Calculations. *J. Phys. Chem. A* **1999**, *103* (49), 10489−10505.
(93) Leo, K.; Wegener, M.; Shah, J.; Chemla, D. S.; Göbel, E. O.; Damen, T. C.; Schmitt-Rink, S.; Schäfer, W. Effects of Coherent Polarization Interactions on Time-Resolved Degenerate Four-Wave Mixing. *Phys. Rev. Lett.* **1990**, *65* (11), 1340−1343.
(94) Bittner, T.; Irrgang, K.-D.; Renger, G.; Wasielewski, M. R. Ultrafast Excitation Energy Transfer and Exciton-Exciton Annihilation Processes in Isolated Light Harvesting Complexes of Photosystem II (LHC II) from Spinach. *J. Phys. Chem.* **1994**, *98* (46), 11821−11826.
(95) DelPo, C. A.; Kudisch, B.; Park, K. H.; Khan, S.-U.-Z.; Fassioli, F.; Fausti, D.; Rand, B. P.; Scholes, G. D. Polariton Transitions in Femtosecond Transient Absorption Studies of Ultrastrong Light−Molecule Coupling. *J. Phys. Chem. Lett.* **2020**, *11* (7), 2667−2674.
(96) Brüggemann, B.; Kjellberg, P.; Pullerits, T. Non-Perturbative Calculation of 2D Spectra in Heterogeneous Systems: Exciton Relaxation in the FMO Complex. *Chem. Phys. Lett.* **2007**, *444* (1), 192−196.
(97) Anda, A.; Cole, J. H. Two-Dimensional Spectroscopy beyond the Perturbative Limit: The Influence of Finite Pulses and Detection Modes. *J. Chem. Phys.* **2021**, *154* (11), 114113.
(98) Zhang, P.-P.; Eisfeld, A. Non-Perturbative Calculation of Two-Dimensional Spectra Using the Stochastic Hierarchy of Pure States. *J. Phys. Chem. Lett.* **2016**, *7* (22), 4488−4494.
(99) Rose, P. A.; Krich, J. J. Automatic Feynman Diagram Generation for Nonlinear Optical Spectroscopies and Application to Fifth-Order Spectroscopy with Pulse Overlaps. *J. Chem. Phys.* **2021**, *154* (3), No. 034109.
(100) Do, T. N.; Chen, L.; Belyaev, A. K.; Tan, H.-S.; Gelin, M. F. Pulse-Shape Effects in Fifth-Order Multidimensional Optical Spectroscopy. *Chem. Phys.* **2018**, *515*, 119−128.
(101) Süß, J.; Engel, V. Exciton−Exciton Annihilation in a Molecular Trimer: Wave Packet Dynamics and 2D Spectroscopy. *J. Chem. Phys.* **2020**, *153* (16), 164310.
(102) Rose, P. A.; Krich, J. J. Efficient Numerical Method for Predicting Nonlinear Optical Spectroscopies of Open Systems. *J. Chem. Phys.* **2021**, *154* (3), No. 034108.
(103) Engel, V. Excitation of Molecules with Ultrashort Laser Pulses: Exact Time-Dependent Quantum Calculations. *Comput. Phys. Commun.* **1991**, *63* (1), 228−242.
(104) Tanimura, Y.; Maruyama, Y. Gaussian−Markovian Quantum Fokker−Planck Approach to Nonlinear Spectroscopy of a Displaced Morse Potentials System: Dissociation, Predissociation, and Optical Stark Effects. *J. Chem. Phys.* **1997**, *107* (6), 1779−1793.
(105) Meyer, S.; Schmitt, M.; Materny, A.; Kiefer, W.; Engel, V. Simulation of Femtosecond Time-Resolved Four-Wave Mixing Experiments on I2. *Chem. Phys. Lett.* **1999**, *301* (3), 248−254.
(106) Gelin, M. F.; Egorova, D.; Domcke, W. Efficient Method for the Calculation of Time- and Frequency-Resolved Four-Wave Mixing Signals and Its Application to Photon-Echo Spectroscopy. *J. Chem. Phys.* **2005**, *123* (16), 164112.
(107) Cheng, Y.-C.; Lee, H.; Fleming, G. R. Efficient Simulation of Three-Pulse Photon-Echo Signals with Application to the Determination of Electronic Coupling in a Bacterial Photosynthetic Reaction Center. *J. Phys. Chem. A* **2007**, *111* (38), 9499−9508.
(108) Renziehausen, K.; Marquetand, P.; Engel, V. On the Divergence of Time-Dependent Perturbation Theory Applied to Laser-Induced Molecular Transitions. *J. Phys. B: At. Mol. Opt. Phys.* **2009**, *42* (19), No. 195402.
(109) Tanimura, Y. Reduced Hierarchy Equations of Motion Approach with Drude plus Brownian Spectral Distribution: Probing Electron Transfer Processes by Means of Two-Dimensional Correlation Spectroscopy. *J. Chem. Phys.* **2012**, *137* (22), 22A550.
(110) Yuen-Zhou, J.; Krich, J. J.; Kassal, I.; Johnson, A. S.; Aspuru-Guzik, A. *Ultrafast Spectroscopy*, 1st ed.; IOP Publishing: Bristol, 2014.
(111) Cina, J. A.; Kovac, P. A.; Jumper, C. C.; Dean, J. C.; Scholes, G. D. Ultrafast Transient Absorption Revisited: Phase-Flips, Spectral Fingers, and Other Dynamical Features. *J. Chem. Phys.* **2016**, *144* (17), 175102.
(112) Smallwood, C. L.; Autry, T. M.; Cundiff, S. T. Analytical Solutions to the Finite-Pulse Bloch Model for Multidimensional Coherent Spectroscopy. *J. Opt. Soc. Am. B, JOSAB* **2017**, *34* (2), 419−429.
(113) Perlík, V.; Hauer, J.; Šanda, F. Finite Pulse Effects in Single and Double Quantum Spectroscopies. *JOSA B* **2017**, *34* (2), 430−439.
(114) Do, T. N.; Gelin, M. F.; Tan, H.-S. Simplified Expressions That Incorporate Finite Pulse Effects into Coherent Two-Dimensional Optical Spectra. *J. Chem. Phys.* **2017**, *147* (14), 144103.
(115) Rose, P. A.; Krich, J. J. Numerical Method for Nonlinear Optical Spectroscopies: Ultrafast Ultrafast Spectroscopy. *J. Chem. Phys.* **2019**, *150* (21), 214105.
(116) Sun, Y.; Yoon, Y.; Steger, M.; Liu, G.; Pfeiffer, L. N.; West, K.; Snoke, D. W.; Nelson, K. A. Direct Measurement of Polariton−Polariton Interaction Strength. *Nat. Phys.* **2017**, *13* (9), 870−875.
(117) Giura, P.; Paulatto, L.; He, F.; Lobo, R. P. S. M.; Bosak, A.; Calandrini, E.; Paolasini, L.; Antonangeli, D. Multiphonon Anharmonicity of MgO. *Phys. Rev. B* **2019**, *99* (22), No. 220304.
(118) Goodwin, H.; Jellicoe, T. C.; Davis, N. J. L. K.; Böhm, M. L. Multiple Exciton Generation in Quantum Dot-Based Solar Cells. *Nanophotonics* **2018**, *7* (1), 111−126.
(119) Klimov, V. I.; Mikhailovsky, A. A.; McBranch, D. W.; Leatherdale, C. A.; Bawendi, M. G. Quantization of Multiparticle Auger Rates in Semiconductor Quantum Dots. *Science* **2000**, *287* (5455), 1011−1013.
(120) Abramavičius, D. Revealing a Full Quantum Ladder by Nonlinear Spectroscopy. *Lith. J. Phys.* **2020**, *60* (3), 154 DOI: 10.3952/physics.v60i3.4302.
(121) Zhang, Z.; Wells, K. L.; Tan, H.-S. Purely Absorptive Fifth-Order Three-Dimensional Electronic Spectroscopy. *Opt. Lett.* **2012**, *37* (24), 5058−5060.
(122) Spencer, A. P.; Hutson, W. O.; Harel, E. Quantum Coherence Selective 2D Raman−2D Electronic Spectroscopy. *Nat. Commun.* **2017**, *8*, 14732.
(123) Malý, P.; Brixner, T. Fluorescence-Detected Pump−Probe Spectroscopy. *Angew. Chem., Int. Ed.* **2021**, *60* (34), 18867−18875.
(124) Selle, R.; Vogt, G.; Brixner, T.; Gerber, G.; Metzler, R.; Kinzel, W. Modeling of Light-Matter Interactions with Neural Networks. *Phys. Rev. A* **2007**, *76* (2), No. 023810.
(125) Selle, R.; Brixner, T.; Bayer, T.; Wollenhaupt, M.; Baumert, T. Modelling of Ultrafast Coherent Strong-Field Dynamics in Potassium

with Neural Networks. *J. Phys. B: At. Mol. Opt. Phys.* **2008**, *41* (7), No. 074019.
(126) Rodríguez, M.; Kramer, T. Machine Learning of Two-Dimensional Spectroscopic Data. *Chem. Phys.* **2019**, *520*, 52−60.
(127) Assion, A.; Baumert, T.; Bergt, M.; Brixner, T.; Kiefer, B.; Seyfried, V.; Strehle, M.; Gerber, G. Control of Chemical Reactions by Feedback-Optimized Phase-Shaped Femtosecond Laser Pulses. *Science* **1998**, *282* (5390), 919−922.
(128) Meshulach, D.; Silberberg, Y. Coherent Quantum Control of Two-Photon Transitions by a Femtosecond Laser Pulse. *Nature* **1998**, *396* (6708), 239−242.
(129) Tiwari, V.; Matutes, Y. A.; Gardiner, A. T.; Jansen, T. L. C.; Cogdell, R. J.; Ogilvie, J. P. Spatially-Resolved Fluorescence-Detected Two-Dimensional Electronic Spectroscopy Probes Varying Excitonic Structure in Photosynthetic Bacteria. *Nat. Commun.* **2018**, *9* (1), 4219.
(130) Pres, S.; Huber, B.; Hensen, M.; Fersch, D.; Schatz, E.; Friedrich, D.; Lisinetskii, V.; Pompe, R.; Hecht, B.; Pfeiffer, W.; Brixner, T. Detection of a Plasmon-Polariton Quantum Wave Packet. *Nat. Phys.* **2023**, *19*, 656−662.
(131) Li, D.; Titov, E.; Roedel, M.; Kolb, V.; Goetz, S.; Mitric, R.; Pflaum, J.; Brixner, T. Correlating Nanoscale Optical Coherence Length and Microscale Topography in Organic Materials by Coherent Two-Dimensional Micro-Spectroscopy. *Nano Lett.* **2020**, *20* (9), 6452−6458.
(132) Stolte, M.; Hecht, R.; Xie, Z.; Liu, L.; Kaufmann, C.; Kudzus, A.; Schmidt, D.; Würthner, F. Crystal Engineering of 1D Exciton Systems Composed of Single- and Double-Stranded Perylene Bisimide J-Aggregates. *Adv. Optical Mater.* **2020**, *8* (18), No. 2000926.
(133) Oliver, T. A. A.; Lewis, N. H. C.; Fleming, G. R. Correlating the Motion of Electrons and Nuclei with Two-Dimensional Electronic−Vibrational Spectroscopy. *Proc. Natl. Acad. Sci. U.S.A.* **2014**, *111* (28), 10061−10066.
(134) Gaynor, J. D.; Courtney, T. L.; Balasubramanian, M.; Khalil, M. Fourier Transform Two-Dimensional Electronic-Vibrational Spectroscopy Using an Octave-Spanning Mid-IR Probe. *Opt. Lett., OL* **2016**, *41* (12), 2895−2898.
(135) Courtney, T. L.; Fox, Z. W.; Slenkamp, K. M.; Khalil, M. Two-Dimensional Vibrational-Electronic Spectroscopy. *J. Chem. Phys.* **2015**, *143* (15), 154201.
(136) Joos, E.; Zeh, H. D.; Kiefer, C.; Giulini, D.; Kupsch, J.; Stamatescu, I.-O. *Decoherence and the Appearance of a Classical World in Quantum Theory*; Springer: Berlin, 2003. DOI: 10.1007/978-3-662-05328-7.
(137) Raghavachari, K.; Anderson, J. B. Electron Correlation Effects in Molecules. *J. Chem. Phys.* **1996**, *100* (31), 12960−12973.
(138) Kim, J.; Huxter, V. M.; Curutchet, C.; Scholes, G. D. Measurement of Electron−electron Interactions and Correlations Using Two-Dimensional Electronic Double-Quantum Coherence Spectroscopy. *J. Phys. Chem. A* **2009**, *113* (44), 12122−12133.
(139) Chemla, D. S.; Shah, J. Many-Body and Correlation Effects in Semiconductors. *Nature* **2001**, *411* (6837), 549−557.

https://doi.org/10.1021/acs.jpclett.3c01694
J. Phys. Chem. Lett. 2023, 14, 7556−7573